Alekseyev V.A. Hypotheses of agate formation: Review and critical analysis

Vernadsky Institute of Geochemistry and Analytical Chemistry RAS, Moscow (alekseyev-v@geokhi.ru)

Abstract. A review of the conditions, features and hypotheses of agate formation has shown that most hypotheses have significant disadvantages. The hypothesis of multiple repetition of two stages turned out to be the most justified: the deposition of an amorphous silica layer and its recrystallization into chalcedony. A critical analysis of this hypothesis led to the construction of its own hypothesis, which is better consistent with natural and experimental studies of the properties of agates and host rocks. In the new hypothesis, the solution in the agate cavities is only in the form of films on the walls. SiO_2 supplies from the sites of dissolution of the host rock are carried out by diffusion in a pore solution. SiO_2 deposition on the wall of the agate cavity occurs as a result of distillation caused by predominant evaporation in a thin layer of solution at a solid wall and repeatedly enhanced by wetting the hydrophilic rough wall with a solution. Agate banding occurs in response to fluctuations in the degree of supersaturation in the solution film on the wall of the agate cavity as a result of fluctuations in the supply of silica caused by migration of SiO_2 sources and transport routes, as well as changes in their intensity during the evolution of the hydrothermal system.

Keywords: agate formation, conditions and mechanisms, hypotheses, distillation

Agate (banded silica, SiO_2) has always attracted attention with its unusual beauty and made one think about how they could have formed. In the Table 1 the main results of agate research, important for understanding their genesis, are summarized.

An increase in the stability of silica minerals included in agates coincides with a decrease in their solubility (Fig. 1). The hypotheses (mechanisms) of agate formation (Fig. 2) have disadvantages. Hypothesis 2a cannot explain the formation of inclusions of molten silica (melting point 1600°C) in magma with a temperature of 1100°C. Hypothesis 2b contradicts the data on the extraction of silica for agates from host rocks. Hypotheses 2c and 2d cannot convincingly explain the mechanism of formation of SiO_2 gel in the cavity and the absence of shrinkage cracks during its aging. Let us dwell on the 2e-2f hypothesis in more detail.

According to the hypothesis, dissolved silica diffuses from the pores of the host rock into the cavity and is deposited on the walls in the form of a gel layer, which prevents further diffusion of SiO_2. The gel layer recrystallizes into porous chalcedony, SiO_2 diffusion resumes, etc. The advantage of this hypothesis is the reasonable assumption that the source of silica for agates is the host rock (Tab. 1). The disadvantages of the hypothesis are as follows. The effect of osmosis and SiO_2 gel as a semipermeable membrane has not been proven. The assumption of a higher solubility of SiO_2 in pores is incorrect. Rather, we can expect an inverse relationship, but only for very small pores (Alekseyev, 2019). A higher concentration of SiO_2 in the pore solution is possible for another reason, namely, as a result of the dissolution of the host rocks. For example, the dissolution of basalt in acidic solutions at 50-120°C caused an increase in the concentration of dissolved silica above the solubility of quartz (Tsuzuki, Ogasawara, 1987).

Table 1. Basic properties and conditions of agate formation according to reviews (Godovikov et al., 1987; Götze et al., 2020; Moxon, Palyanova, 2020)

Properties	Detail
Host rocks	Mainly basalts and andesites
Temperature	25-230°C
Composition of solutions	H_2O, CO_2, H_2S, F (mixing of deep and surface waters)
The main composition	Chalcedony (less often quartzine) in fusion with morganite (twisted fibers), quartz (micro-grained in stripes, coarse-grained in the center)
Impurities	Amorphous silica, cristobalite opalite, hematite, calcite, clay minerals, zeolites enrichment with elements of host rocks (Al, Si, Ca, Fe, Na, K)
Types of banding	The stripes are sub-parallel to the walls of the cavities (predominate) horizontal stripes (a rare Uruguayan species)
Reasons for band differences	Phase composition (chalcedony or quartz), size and shape of crystallites, porosity, impurities (usually yellow goethite or red hematite)
Rare textures	Infiltration channels, pseudostalactites, moss textures

This real feature of forming supersaturated solutions could replace in the model (Walger et al., 2009) the controversial statement about the higher solubility of SiO_2 in a pore solution, but even here a number of difficulties arise. On the way to the agate cavity, at least partial deposition of SiO_2 is inevitable, which will cause pore blockage and rapid termination of SiO_2 supplies. Let's say the supply of SiO_2 to the cavity still occurs. Then it is difficult to explain the uniform deposition of silica along the entire wall with the formation of a typical concentric banding for agates. Under these conditions, it is more likely to expect SiO_2 deposition at the bottom of the cavity, as in quite rare Uruguayan agates with horizontal layering. Let's say a gel layer of SiO_2 has formed all over the wall. The aging of this layer should first lead to the formation of microcrystalline opal-C, which has a higher solubility than chalcedony (Fig. 1). Opal-C also has a high porosity, which allows it to be permeable to new SiO_2 supplies, i.e. the process should not reach the stage of chalcedony formation. In this case, agates with layers of opal-C, and not chalcedony, should be formed, which contradicts natural research. Taking into account the above criticisms, the hypothesis (Walger et al., 2009) also does not look realistic.

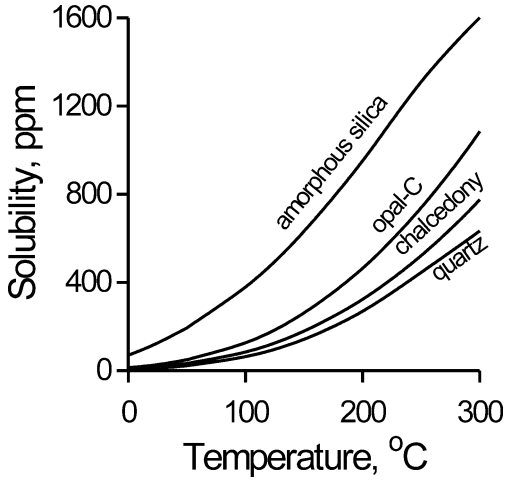

Fig. 1. Temperature dependences of solubility of different modifications of silica in water according to (Plyasunov, 2012; Fournier, 1977).

It is possible to get rid of the shortcomings of the hypothesis (Walger et al., 2009) if we assume that the hydrogeological regime of agate formation corresponds to the conditions of an unsaturated porous medium, i.e. an aqueous solution completely fills only small pores, and in large pores it is present in the form of films together with water vapor. Such stagnant zones are usually located on the edge of the main transport routes of hydrothermal solutions. The predominant mechanisms of movement of an aqueous solution in an unsaturated porous medium are suction under the action of capillary forces and film transfer under the action of disjoining pressure. These mechanisms are accompanied by adsorption/desorption and evaporation/condensation processes (Wedekind et al., 2013). Under these conditions, the transfer of silica from the place of its transition to the solution to the place of deposition in the agate cavity should be provided mainly by diffusion in the pore solution, which is facilitated by the high porosity of the host rock with pores connected to each other. For example, the measured connected porosity of basalts can reach 80% (Moitra, Houghton, 2021).

The proposed mechanism of agate formation is based on the phenomenon of distillation of silica solution in a closed system (Alekseyev, 2023). Distillation is initiated by the predominant evaporation of water from a thin layer of solution near a solid wall and is amplified many times during the propagation of this layer along a rough hydrophilic wall as a result of wetting. Figure 3 shows a diagram of this phenomenon in relation to the growth of chalcedony in agates. In this case, the supersaturation of the solution necessary for the deposition of silica is created on site, and the transport of SiO_2 to the agate cavity can be carried out in low concentrations, which reduces the risk of silica deposition in the pores and pore blockage. The approach to the equilibrium of the solution with chalcedony from low concentrations prevents the formation of amorphous silica (Fig. 1). Therefore, periodic containment of SiO_2 supplies into the cavity by a layer of amorphous silica becomes questionable. Another explanation of the reason for the formation of agate banding is needed, i.e. the change in texture from layer to layer.

The texture of the agate layer (shape, size and orientation of quartz or chalcedony crystals, porosity) is determined by the degree of supersaturation of the film solution, which depends on the balance of outflow and inflow of SiO_2. The inflow of SiO_2 to the agate cavity from different sides cannot be homogeneous due to the initial heterogeneity of the host rock in composition and pore distribution. This heterogeneity may change during hydrothermal changes of the host rock. Silica may partially precipitate, and the dissolution of the host rock may lead to the appearance of new pores and/or to an increase in old ones. All this can lead to the blocking of some and the appearance of other transport routes. Variations in the supply of SiO_2 to agate may also be associated with changes in the hydrogeological regime. The distribution of the solution in an unsaturated porous medium reacts sensitively to changes in pressure, temperature and composition of the solution, which, in turn, is determined by the peculiarities of the evolution of the hydrothermal system. As a result, the areas of preferential SiO_2

extraction into the solution and the main routes of SiO_2 transport can migrate, causing fluctuations in the rate of SiO_2 diffusion delivery to the agate cavity and the degree of supersaturation in the solution film on the cavity wall. Similar fluctuations in external factors cause the formation of annual tree rings. A low rate of SiO_2 diffusion in the host rock in any area near the agate cavity (for example, due to low local porosity) can cause a local decrease in the thickness of the agate layers next to this area until they are completely wedged out. This reason may be an alternative explanation of the mechanism of formation of "infiltration channels".

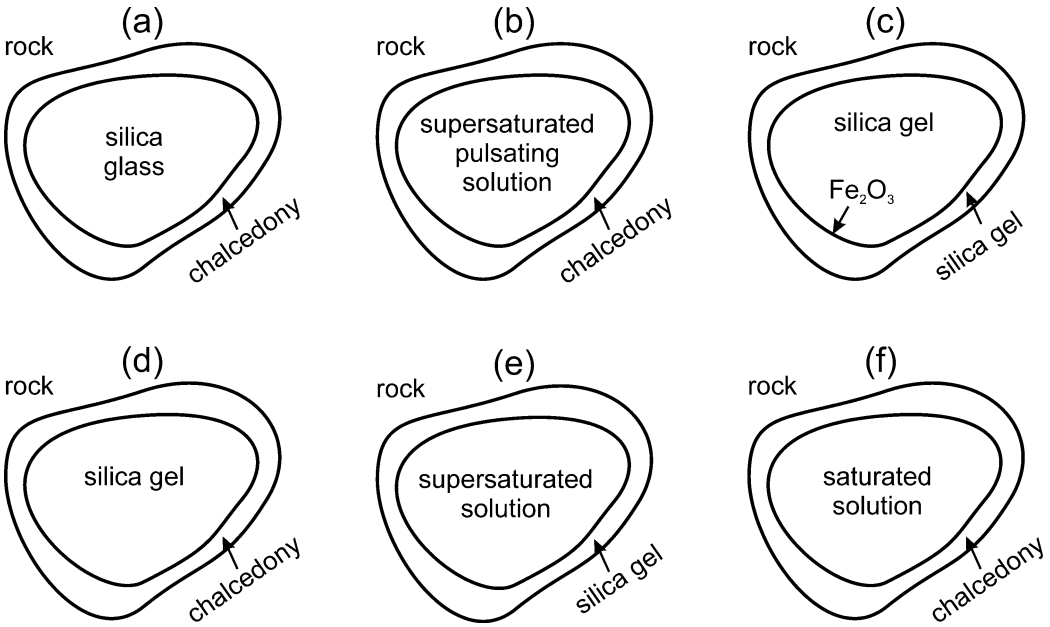

Fig. 2. Diagrams of the previously proposed mechanisms of agate formation (only the first layer is shown): (a) crystallization of quartz glass inclusions (Nacken, 1948); (b) precipitation of silica from a pulsating solution (Flörke et al., 1982); (c) self-organization of a lump of SiO_2 gel into Liesegang rings (Liesegang, 1915); (d) self-organization of a gel lump during recrystallization (Wang, Merino, 1990); (e)-(f) layered deposition of silica gel (e) followed by its recrystallization into chalcedony (f) (Walger et al., 2009).

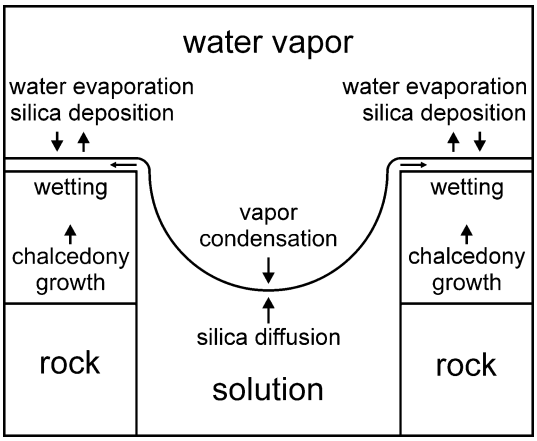

Fig. 3. Diagram of the proposed mechanism of chalcedony growth in agates. At the entrance to the agate cavity, the solution spreads along the wall, forming a thin film. The water from the film evaporates, which leads to the deposition of SiO_2. Excess water vapor condenses on the meniscus, diluting the SiO2 solution. This dilution is compensated by the diffusion of SiO2 from the dissolution sites of the host rock. The decrease in the amount of water in the film is compensated by the supply of a solution from the meniscus.

Long-term supplies of silica during the formation of agates are provided by irreversible reactions of transformation of primary minerals (plagioclases, pyroxenes, amphiboles) into secondary minerals (kaolinite, zeolite, calcite, Fe oxides) with the transition of SiO_2 into solution. In such reactions, there is no restriction associated with achieving the equilibrium of the mineral with the solution, since primary minerals formed in the magmatic process usually become unstable at lower temperatures of the hydrothermal process and must completely turn into secondary ones. The above features of the proposed hypothesis are given in Table 2.

The lack of experimental data on the synthesis of agates can be made up using the above model and taking into account the fact that lava icicles protruding into the agate cavity also undergo hydrothermal changes and become overgrown with banded chalcedony, forming pseudostalactites (Godovikov et al., 1987). An analogy of such a situation in experiments can be a cylinder of porous andesite or basalt placed in an autoclave with water

so that the upper part of the cylinder protrudes above the water. According to experimental data (Okamoto et al., 2010), the maximum temperature for the synthesis of agate should not exceed 300 °C. The duration of experiments at this temperature can reach many years to obtain at least several strips of agate.

Table 2. Features of the proposed hypothesis of agate formation

Processes or objects	Specifications
The state of the solution	In agate cavities and in large pores, the solution is in the form of films on the walls, medium and small pores are partially or completely filled with the solution
Migration of solution in pores	Under the action of capillary forces and disjoining pressure during fluctuations of T and P, with a change in the distribution of pores in the dissolution / precipitation processes
The transition of silica into solution	Irreversible reactions of transformation of host rocks into secondary minerals
Silica transport	Diffusion in a pore solution
Deposition of SiO_2 on the wall of the agate cavity	As a result of distillation caused by predominant evaporation in a thin layer of solution at a solid wall and repeatedly enhanced by wetting of a hydrophilic rough wall with a solution
Causes of concentric banding of agates	Fluctuations in the degree of supersaturation in the solution film on the wall of the agate cavity as a result of fluctuations in the supply of silica caused by the migration of sources and transport routes of SiO_2, as well as changes in their intensity during the evolution of the hydrothermal system

References

Alekseyev V.A. Spontaneous solution distillation in a closed silica-water system at the water-vapor interface: Review of experimental studies // Advances in Geochemistry, Analytical Chemistry, and Planetary Sciences. (eds. V.P. Kolotov and N.S. Bezaeva). Springer, 2023. P. 175-186.

Alekseyev V.A. Nanoparticles and nanofluids in water–rock interactions // Geochem. Int. 2019. Vol. 57. No 4. P. 357-368.

Flörke O.W., Köhler-Herbertz B., Langer K., Tönges I. Water in microcrystalline quartz of volcanic origin: Agates // Contr. Mineral. Petrol. 1982. Vol. 80. No 4. P. 324-333.

Fournier R.O. Chemical geothermometers and mixing models for geothermal systems // Geothermics. 1977. Vol. 5. No 1-4. P. 41-50.

Godovikov A. A., Ripinen O. I., Motorin S. G. Agates. Moscow, Nedra, 1987.

Götze J., Möckel R., Pan Y. Mineralogy, geochemistry and genesis of agate—a review // Minerals. 2020. Vol. 10. No 11. art. 1037.

Liesegang R. E. Die Achate. Verlag von Theodor Steinkopff, Dresden und Leipzig, 1915.

Moitra, P., Houghton, B.F. Porosity-permeability relationships in crystal-rich basalts from Plinian eruptions // Bull. Volcanol. 2021. Vol. 83. No 11. art. No 71.

Moxon T., Palyanova G. Agate genesis: A continuing enigma // Minerals. 2020. Vol. 10. No 11. art. 953.

Nacken R. (1948) Über die Nachbildung von Chalcedon-Mandeln // Natur und Volk. 1948. Vol. 78. P. 2-8.

Okamoto A., Saishu H., Hirano N., Tsuchiya N. Mineralogical and textural variation of silica minerals in hydrothermal flow-through experiments: Implications for quartz vein formation // Geochim. Cosmochim. Acta. 2010. Vol. 74. No 13. P. 3692-3706.

Plyasunov A.V. Thermodynamics of $Si(OH)_4$ in the vapor phase of water: Henry's and vapor–liquid distribution constants, fugacity and cross virial coefficients // Geochim. Cosmochim. Acta. 2012. Vol. 77. P. 215-231.

Tsuzuki Y., Ogasawara K. Dissolution experiments on albite and basalt glasses at various temperatures and their application to hydrothermal alteration in geothermal fields // Geochem. J. 1987. Vol. 21. No 6. P. 261-281.

Walger E., Mattheß G., Von Seckendorff V., Liebau F. The formation of agate structures: Models for silica transport, agate layer accretion, and for flow patterns and flow regimes in infiltration channels // Neues Jahrb. Mineral. Abh. 2009. Vol. 186. No 2. P. 113-152.

Wang Y., Merino E. Self-organizational origin of agates: Banding, fiber twisting, composition, and dynamic crystallization model // Geochim. Cosmochim. Acta. 1990. Vol. 54. No 6. P. 1627-1638.

Wedekind W., López-Doncel R., Dohrmann R., Kocher M. Weathering of volcanic tuff rocks caused by moisture expansion // Environ. Earth Sci. 2013. Vol. 69. No 1203-1224.

Korzhinskaya V.S., Kotova N.P. The problem of hydrothermal mass transfer and deposit of tantalum and niobium during the formation of their deposits (according to experimental data)

Korzhinskii Institute of Experimental Mineralogy RAS
vkor@iem.ac.ru; kotova@iem.ac.ru

Abstract. Experimental data on the solubility of columbite (Mn, Fe) (Nb, Ta)$_2$ O$_6$, pyrochlore (Ca, Na)$_2$(Nb, Ta)$_2$O$_6$(O, OH, F), tantalum oxides (Ta_2O_5) and niobium (Nb_2O_5) in

acidic, neutral and alkaline aqueous solutions: fluoride, chloride, mixed (mHF + mHCl), carbonate Na_2CO_3 and (Na_2CO_3 + NaF), alkaline NaOH and (NaOH + NaF) in the concentration range from 0.01 to 2.0 mol/kg H_2O at a temperature of 300 – 550°C, a pressure of 50 - 100 MPa at $f(O_2)$ given by Co-CoO and Ni-NiO buffers have been obtained. It has been established that the solubility of the minerals pyrochlore and columbite is incongruent, while the solubility of pyrochlore is higher than that of columbite. The presence of the F-ion has a positive effect on the solubility of minerals and oxides, and the complex formation of Nb is much more pronounced than that of Ta. The role of temperature and pressure is secondary.

Keywords: experiment, solubility, pyrochlore, columbite, tantalum and niobium oxides, fluid, physicochemical conditions

To obtain quantitative estimates of the possibility of hydrothermal transport and deposition of tantalum and niobium under physicochemical conditions characteristic of the formation of the main types of endogenous deposits of these metals associated with "apogranites", pegmatites, alkaline metasomatites, alkaline syenites and carbonatites, we carry out systematic experimental studies of the solubility of columbite-tantalite ((Mn, Fe) (Nb, $Ta)_2$ O_6, pyrochlore (Ca, $Na)_2$ (Nb, $Ta)_2O_6$(O, OH, F), tantalum (Ta_2O_5) and niobium (Nb_2O_5) oxides in acidic , neutral and alkaline aqueous solutions: fluoride, chloride, mixed (mHF + mHCl), carbonate Na_2CO_3 and (Na_2CO_3 + NaF), alkaline NaOH and (NaOH + NaF) in the concentration range from 0.01 to 2.0 mol / kg H_2O at a temperature of 300 – 550°C, a pressure of 50 - 100 MPa and an oxygen fugacity $f(O_2)$ specified by Co-CoO and Ni-NiO buffers.

The experiments were carried out on a high-pressure hydrothermal unit using the ampoule technique, which makes it possible to use solid-phase oxygen buffers isolated from the reagents. Fragments of natural single crystals of pyrochlore from the weathering crusts of the Tatarka carbonatite deposit and columbite from the Ulug Tanzek deposit (Eastern Sayan Mountains), as well as tantalum and niobium oxides, chemical reagents Ta_2O_5 and Nb_2O_5, which are the analogues of the rare minerals tantite and nioboxide, were used in the experiments. The choice of simple oxides of Ta and Nb is due to the fact that their solubility limits the upper limit of the concentration of these elements in hydrothermal solutions, since mineral phases of tantalum-niobates of a more complex composition (columbite, pyrochlore, and others), which are stable under natural conditions, have a lower solubility than oxides. Solution concentrations varied within 0.01m – 2m. Run duration was 15-30 days.

After the runs, the solid products were separated from the solutions by centrifugation. To control congruent or incongruent dissolution of Nb oxide and to determine chemical composition of newly-formed phases (in case of their detection) the initial materials and solid run products were studied by X-ray diffraction, and electron microprobe analysis (Cam Scan MV 2300 (VEGA TS5130MM).

The quenched aqueous solutions were then analyzed using ICP/MS (Inductively Coupled Plasma Mass Spectrometry) and ICP/AES (Atomic Emission Spectroscopy) for Nb, Ta, Mn, and Fe and admixture elements Ti, W, and Sn.

The results of the study of pyrochlore and niobium oxide solubility in fluoride and chloride solutions (HF, HCl, KF, KCl) at 550°C and 100 MPa are shown in (Fig. 1 and 2). It has been established that in HF and KF solutions the dependence of niobium solubility on the fluorides concentration is positive for both pyrochlore and Nb_2O_5. In the range of low HF concentrations (0.01m), the maximum niobium content for Nb_2O_5 is $n \times 10^{-4}$ m, and for pyrochlore n $\times 10^{-6}$ m. In the region of high HF concentrations (1.0 m and above), the niobium content increases and it is $n \times 10^{-0.5}$ m for Nb_2O_5 and pyrochlore. A similar picture is observed in KF solutions. As shown by experimental studies (Zaraisky et al., 2010; Korzhinskaya et al., 2012; 2014), in all chloride solutions, both at low and high chloride concentrations, the niobium solubility is lower than in fluoride solutions. The niobium content for pyrochlore increases by only an order of magnitude with increasing HCl concentration, and it is more than an order of magnitude higher than for niobium oxide, which can be explained by the high solubility of sodium and calcium present in pyrochlore. For pyrochlore, as the KCl concentration increases, the Nb content in the solution increases, but remains three orders of magnitude lower than its solubility in HCl solutions. At the same time, the Nb_2O_5 solubility in KCl solutions of low concentrations is of the same order as in HCl solutions, and in 1 and 2 m HCl solutions it is an order of magnitude lower, due to the incongruent solubility of niobium oxide in these solutions. However, compared with pyrochlore, the niobium oxide solubility in the region of KCl low solution concentrations remains higher by 2 orders of magnitude, and one order of magnitude higher in the region of high concentrations of KCl. The obtained data confirm the thesis that the solubility of simple oxides (Ta_2O_5, Nb_2O_5) limits the upper limit of the concentration of these elements in hydrothermal solutions.

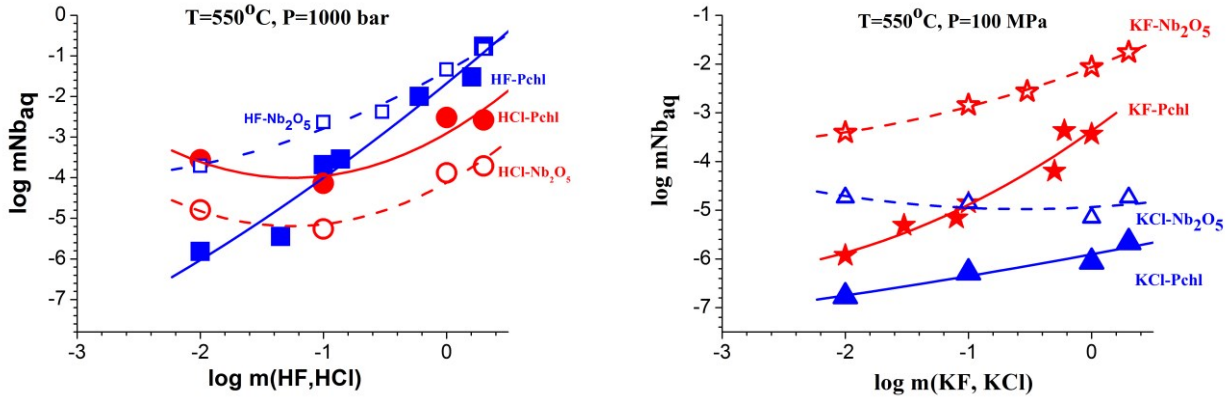

Fig. 1. Concentration dependence of the niobium content during the dissolution of pyrochlore and Nb_2O_5 in HF and HCl solutions at T = 550°C and P = 100 MPa (Co-CoO buffer)

Fig. 2. Concentration dependence of the niobium content during the dissolution of pyrochlore and Nb_2O_5 in KF and KCl solutions at T = 550°C and P = 100 MPa (Co-CoO buffer)

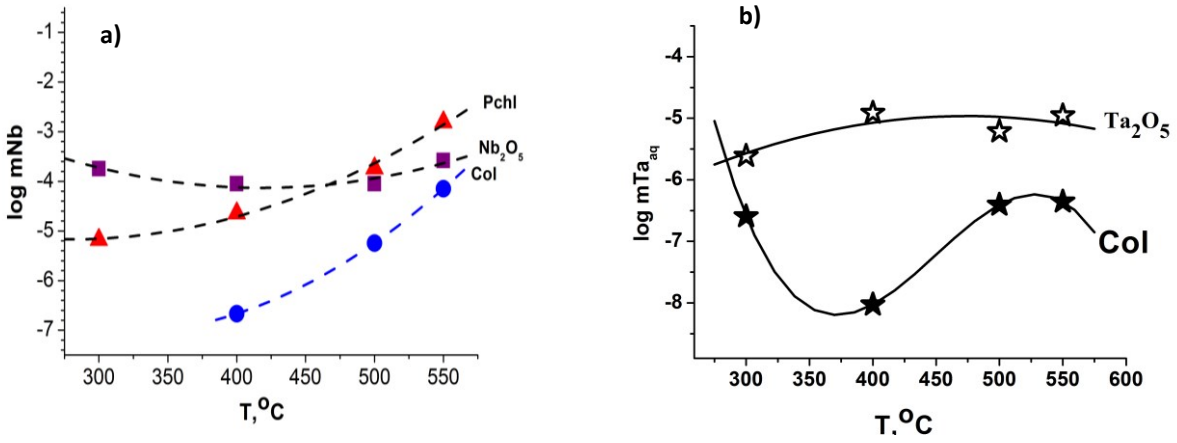

Fig 3a. Temperature dependence of the equilibrium content of niobium during the dissolution of Nb_2O_5, pyrochlore (Pchl) and columbite (col) in (0.1m HF + 0.5m HCl) solution, (Co-CoO buffer)

Fig. 3b. Temperature dependence of the equilibrium content of tantalum during the dissolution of Ta_2O_5 and columbite (col) in (0.1m HF + 0.5m HCl) solution, (Co-CoO buffer)

The concentration and temperature dependences of the columbite-tantalite, pyrochlore, tantalum and niobium oxides solubility in fluoride-chloride aqueous solutions (mHF + mHCl) at 300–550°C, 100 MPa (Co–CoO buffer) were experimentally studied (Korzhinskaya, Kotova, 2016; Kotova et al., 2022). The HF concentration varied from 0.01 m to 2 m, while the HCl concentration remained constant at 0.5 m. A comparative analysis of the equilibrium contents of niobium and tantalum during the dissolution of niobium and tantalum oxides, pyrochlore and columbite-tantalite in fluoride, chloride and mixed fluoride-chloride solutions showed that at 550°C, 100 MPa, the addition of Cl-ion to fluoride solutions reduces the equilibrium content of niobium and tantalum by approximately 1–1.5 orders of magnitude (Kotova et al. 2022).

The experimental studies carried out did not reveal clearly defined unambiguous dependences of the temperature influence on the solubility of Nb and Ta compounds in (mHF + 0.5 mHCl) solutions of different concentrations (Fig. 3a and Fig. 3b). For pyrochlore and columbite a positive temperature dependence is observed for niobium.

It has been established that when Nb_2O_5 is dissolved in (0.1 mHF + 0.5 mHCl) solutions at 300°C and 100 MPa, the equilibrium content of niobium is 1.5 orders of magnitude higher than that of pyrochlore and 3.5 orders of magnitude higher than that of columbite, and is $n \times 10^{-4}$ m (Fig. 3a). A change in temperature does not significantly affect the solubility of niobium oxide in (0.1 mHF + 0.5 mHCl) solutions, while for pyrochlore and columbite.a positive temperature dependence is observed. An analysis of the experimental data obtained in studying the temperature dependences of

the equilibrium contents of tantalum upon dissolution of Ta_2O_5 and columbite in a (0.1 mHF + 0.5 mHCl) fluid showed that, upon dissolution of Ta_2O_5 in a (0.1 mHF + 0.5 mHCl) solution, the tantalum content is $n \times 10^{-5}$ m. Moreover, the temperature has little effect on the solubility of tantalum oxide. When dissolving columbite in a (0.1 mHF + 0.5 mHCl) solution at 300, 500, and 550°C and 100 MPa, the tantalum content is almost the same and amounts to $n \times 10^{-6.5}$ m, which is 1.5 orders of magnitude lower than for Ta_2O_5. At 400°C, the equilibrium content of tantalum is minimal ($n \times 10^{-8}$ *m*), which is associated with the formation of a solid phase with the composition Mn_2TaO_3 in the solution (Fig. 3b).

According to the obtained experimental data on the solubility of natural minerals pyrochlore and columbite, as well as oxides of Ta and Nb in carbonate and alkaline solutions at 300 - 550 ° C and 50 - 100 MPa (buffers Co-CoO and Ni-NiO), it was found that the solubility of pyrochlore and columbite minerals has an incongruent character, while the solubility of pyrochlore is higher than the solubility of columbite (Korzhinskaya and Kotova, 2011; 2017). The experiments carried out to study the pressure effect on the solubility of pyrochlore and columbite in alkaline solutions at 50 and 100 MPa showed that in NaOH solutions, the solubility of pyrochlore increases by an order of magnitude with increasing pressure at all temperatures. In a 1m Na_2CO_3 solution only at 300°C this dependence is violated due to the formation of new phases with niobium. (Fig. 4 and 5) shows the concentration dependences of the tantalum content during the dissolution of pyrochlore, columbite, tantalum oxide in Na_2CO_3 solutions (Fig. 4) and the niobium content during the dissolution of pyrochlore, columbite and niobium oxide in NaOH solutions (Fig. 5).

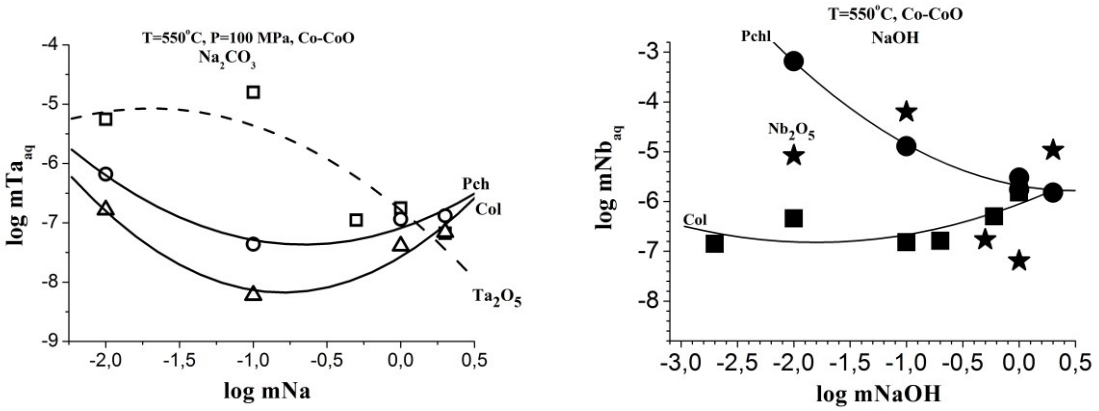

Fig. 4. Concentration dependence of tantalum content during the dissolution of pyrochlore, columbite and Ta_2O_5 in Na_2CO_3 solutions at T=550°C and P=100 MPa (Co-CoO buffer)

Fig. 5. Concentration dependence of niobium content during the dissolution of pyrochlore, columbite and Nb_2O_5 in NaOH solutions at T=550°C and P=100 MPa (Co-CoO buffer)

The results of the studies performed show that the transfer of Ta and Nb is possible only with sufficiently high concentration fluoride solutions, mainly HF and KF solutions. Chloride and carbonate hydrothermal solutions, due to the very low solubility of tantalum-niobates, close to the limit of detection, apparently are not able to transport these metals in the quantities necessary to form their industrial concentrations. However, it can be assumed that during the long-term evolution of the fluid-magmatic system, hydrothermal transport and concentration of Nb by sodium carbonate solutions are still possible, since our studies suggest that Nb is more capable to complex formation with Na and Ca in alkaline solutions, while similar Ta complexation is largely suppressed, which is consistent with the selective confinement of Nb deposits to alkaline igneous rocks and carbonatites.

The work was carried out on the topic: FMUF-2022-0003 and with the support of the Russian Foundation for Basic Research (grants10-05-00292; 11-05-01185;14-05-00424;15-05-03393)

References

1. Korzhinskaya V. S., Kotova N. P. and Corresponding member of the RAS Shapovalov Yu.B. Experimental Study of Manganese Tantalite and Ta_2O_5 Solubility in Chloride Solutions // Doklady Earth Sciences. 2014. V. 459. N. 1. P. 1409–1412
2. Korzhinskaya V.S., Kotova N.P. Experimental modeling of possibility of hydrothermal transferring niobium by fluoride // In: Electron Sci Inform J "Vestnik Otdelenia nauk Zemle RAN". 2012. V. 4, NZ9001. doi:10.2205/2012NZ_ASEMPG

3. Korzhinskaya V. S., Kotova N. P. and Corresponding member of the RAS Shapovalov.Yu. B. Experimental Study of Natural Pyrochlore and Niobium Oxide Solubility in Alkaline Hydrothermal Solutions// Doklady Earth Sciences. 2017. V. 475. N.1. P. 793–796.
4. Korzhinskaya V. S., Kotova N. P. Comparison of data on the solubility of columbite, pyrochlore and oxides of Ta and Nb in alkaline aqueous solutions at T = 550°C, P = 1000 bar (Co-CoO buffer) // In: Electron Sci Inform J "Vestnik Otdelenia nauk o Zemle RAN". 2011. V. 3. NZ6043. doi:10.2205/2011NZ000173.
5. Kotova, N.P., Korzhinskaya, V.S. and Corresponding member of the RAS Shapovalov Yu.B. Experimental Study of the Solubility of Natural Tantalite and Pyrochlore and Tantalum and Niobium Oxides in Hydrothermal Fluoride–Chloride Solutions // Doklady Earts Sciences. 2022. V. 505. N.1. P. 431-438
6. Korzhinskaya V.S., Kotova N.P. Experimental study of fluid composion (HF+HCl) influence on niobium behavior when dissolving pyrochlore and niobium oxide at T = 550 ° C, P = 1000 bar (Co-CoO buffer) // Experiment in Geosciences. 2016. V. 22. N.1. P. 61-63.
7. Zaraisky G.P., Korzhinskaya V.S., Kotova NP. Experimental studies of Ta_2O_5 and columbite-tantalite solubility in fluoride solutions from 300 to 550°C and 50 to 100 MPa// J.Mineral and Petrol. 2010. V. 99. N. 3/4. P. 287–300

Kotova N.P. Experimental study of the effect of fluoride concentration and fluid pressure on Nb_2O_5 solubility.

Korzhinskii Institute of Experimental Mineralogy RAS
kotova@iem.ac.ru

Abstract. The effect of fluoride concentration and fluid pressure on the niobium oxide solubility at T = 550°C and P = 50, 100, 200 and 500MPa in NaF solutions with concentrations of 0.1 and 1.0 m was experimentally studied. It was found that with an increase in pressure from 50 to 200 MPa, the Nb content in 0.1 m NaF solutions decreases by 0.5 orders of magnitude, and in 1 m NaF solutions the Nb content increases by 0.5 orders of magnitude. With a further increase in pressure to 500 MPa, the niobium content practically does not change and remains in the range of 10^{-3} mol/kg H_2O in 0.1 m NaF solutions and 10^{-2} mol/kg H_2O in 1 m NaF solutions.

Keywords: experiment, niobium oxide, hydrothermal solubility, pressure, fluoride solutions

This study is within the framework of the fundamental scientific problem of the genesis of rare-metal deposits of tantalum and niobium. The urgency of the problem lies in the need to conduct experimental studies to obtain quantitative estimates of the possibility of hydrothermal transport and deposition of tantalum and niobium under physicochemical conditions typical for the formation of the main types of endogenous deposits of these metals associated with "apogranites", pegmatites, alkaline metasomatites, alkaline syenites and carbonatites.

To this end, we previously studied the solubility of simple and complex oxides of tantalum and niobium in fluoride and chloride solutions in a wide range of temperatures, pressures, oxygen fugacity, cationic composition and concentration of solutions, which is important for tantalum and niobium deposits associated with calc-alkaline, including lithium fluoride granites ("apogranites") (Zaraisky et. al., 2010; Korzhinskaya et al., 2014; Kotova, 2015). Also, the concentration and temperature dependences of the solubility of tantalum, niobium oxides and single crystals of natural columbite and pyrochlore in alkaline and carbonate aqueous solutions, characteristic of deposits of these metals, genetically associated with alkaline granites, alkaline syenites and carbonatites, were studied (Korzhinskaya et al. 2017). It was shown that the hydrothermal transport of Ta and Nb is favored by the participation of acidic fluoride solutions of high concentration (0.1-1.0m) and the reducing environment. It was found that a strong increase in the solubility of tantalum niobates. (by 1.5-2 orders of magnitude) with a decrease in oxygen fugacity from the level of Ni-NiO to Co-CoO buffer can be of fundamental importance for the formation of this type of deposits in "apogranites" due to the high reduction of high-temperature magmatogenic aqueous fluids generated by parent ilmenite type granites. The subsequent increase in oxygen fugacity at the postmagmatic stage in the domes of rare-metal granites can serve as one of the main reasons for the deposition of tantalum-niobates here.

This work is a continuation of experiments on the study of the solubility of mineral phases stable under natural conditions of tantalum-niobates of complex composition (columbite, pyrochlore, etc.), as well as simple oxides of Ta and Nb. The study of the solubility of simple oxides of Ta and Nb is a necessary link in solving the fundamental scientific problem of the genesis of rare-metal deposits of tantalum and niobium, since the more complex composition of natural minerals, which have a lower solubility in Ta and Nb concentrations, makes it difficult to interpret the results thermodynamically.

New data have been obtained on the study of the solubility of niobium oxide (β-Nb_2O_5), an analogue of the rare mineral nioboxide, in 0.1 and 1 m NaF solutions at 550°C, pressures of 50, 100, 200, and 500 MPa, and oxygen fugacity corresponding to the Co - CoO buffer. The run duration was 10-18 days. Experiments at 550 °C and 50 to 100 MPa were performed on a hydrothermal line. A sealed-capsule quench technique was employed. Experiments at 550°C and 200 to 500 MPa were carried out on a

high gas pressure installation with internal heating (gas bomb). It allows reaching pressures up to 6 MPa and temperatures up to 1400 ° C. Run temperatures were measured with an accuracy of ± 5 °C. The pressure was regulated with a maximum uncertainty of ± 5 MPa.

To control congruent or incongruent dissolution of Nb oxide and to determine chemical composition of newly-formed phases (in case of their detection) the initial materials and solid run products were studied by X-ray diffraction, and electron microprobe analysis (Cam Scan MV 2300 (VEGA TS5130MM).

The quenched aqueous solutions were then analyzed using ICP/MS (Inductively Coupled Plasma Mass Spectrometry) and ICP/AES (Atomic Emission Spectroscopy) for Nb, Ta, Mn, and Fe and admixture elements Ti, W, and Sn.

The results of the experiments are presented in Figs. 1 and 2. An analysis of the data obtained showed that in 0.1 m NaF solutions, an increase in fluid pressure from 50 to 200 MPa leads to a decrease in the solubility of niobium oxide by approximately 0.5 orders of magnitude (from n*10-2.2 to n*10-3 m). With a further increase in pressure from 200 to 500 MPa, the solubility of niobium oxide does not change, remaining at the level of n*10-3 m. In 1 m NaF solutions, an increase in fluid pressure from 50 to 200 MPa leads to an increase in the equilibrium content of niobium by 0.5 orders of magnitude (from n*10-2.2 to n*10-1.8 m). However, further, as the fluid pressure increases from 200 to 500 MPa in concentrated 1 m NaF solutions, as well as in low concentration NaF solutions, the equilibrium content of niobium practically does not change, remaining at the level of n*10-1.8. m (Fig. 1).

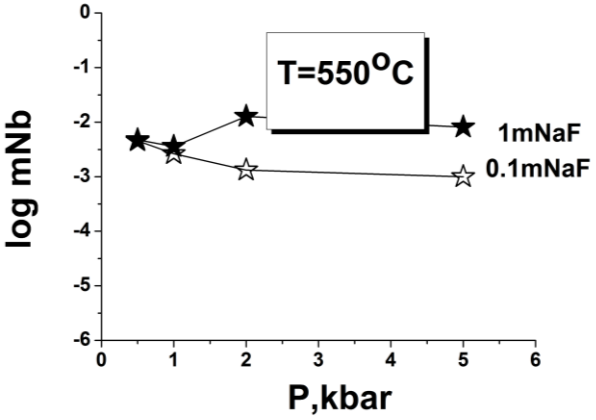

Fig.1. Effect of NaF concentration and fluid pressure on Nb_2O_5 solubility at T=550°C (asterisks – 0.1 m NaF, shaded asterisks – 1 m NaF)

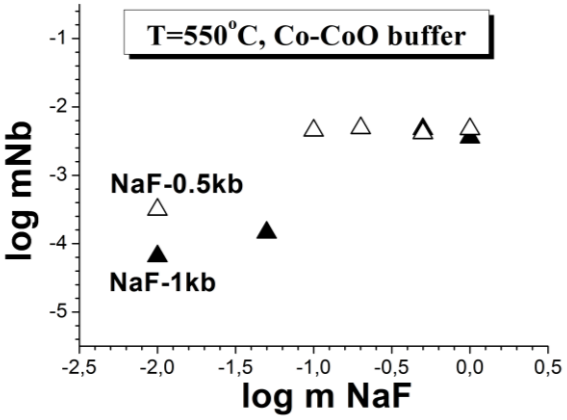

Fig.2. Effect of NaF concentration and fluid pressure on Nb_2O_5 solubility at T=550°C (triangles – at P = 0.5 kbar, shaded triangles – at P = 1 kbar

Comparison of the results of experiments on studying the concentration dependences of the solubility of niobium oxide in NaF solutions at T = 550°C and pressures of 50 and 100 MPa (Kotova, 2012; Kotova, 2014) showed that a decrease in fluid pressure from 100 to 50 MPa in solutions with a low concentration of F – ion (0.01 m NaF solution) leads to an increase in the solubility of Nb_2O_5 by approximately one order of magnitude. In NaF solutions with higher concentrations, the influence of a decrease in fluid pressure ceases to affect the solubility of Nb_2O_5. Starting from a concentration of 0.1 m NaF, the equilibrium content of niobium in the solution has similar values both at 100 and 50 MPa, reaching a value of n*10-2 m, which is quite sufficient for the real mass transfer of niobium by hydrothermal solutions (Fig. 2).

The results of the X-ray phase analysis of the solid products of the experiments showed that niobium oxide dissolves congruently in a 0.01 m NaF solution at T = 550°C and P = 50 MPa. In all other cases, niobium oxide dissolves incongruently. In this case, in 0.1 and 0.2 m NaF solutions, niobium oxide is replaced by sodium oxyfluoride $NaNb_6O_{15}F$, which belongs to the monoclinic system, and in 0.5 and 1 m NaF solutions, crystals of a new phase are formed, which is a structural analog of $Ca_{0.4}H_{1.2} \cdot Nb_2O_5 \cdot H_2O$.

The conducted studies have shown that the experimentally established fact, which is of fundamental importance for understanding the genesis of tantalum and niobium deposits, consists in the fact that the hydrothermal transport of these ore metals in the quantities necessary for the formation of their industrial concentrations is possible only with concentrated fluorine-containing solutions. P-T

conditions have little effect on the solubility of niobium and tantalum.

The work was carried out on the topic: FMUF-2022-0003 and with the support of the Russian Foundation for Basic Research (grant 20-05-00307a)

References

1. Korzhinskaya V.S., Kotova N.P., and Corresponding member of the RAS Shapovalov Yu.B. Experimental study of manganese-tantalite and Ta_2O_5 solubility in chloride solutions // Doklady Earth Sciences. 2014. V. 459. N.1. P. 1409–1412.
2. Korzhinskaya V.S., Kotova N.P., and Corresponding member of the RAS Shapovalov Yu.B. Experimental study of natural pyrochlore and niobium oxide solubility in alkaline hydrothermal solution // Doklady Earth Sciences. 2017. V. 475. N.1. P. 793-796.
3. Kotova N.P. Experimental study of Nb_2O_5 solubility in chloride solutions at 300-550° C and 100 MPa // Experiment in Geosciences.2015. V. 21. N. 1. P. 41
4. Zaraisky G.P., Korzhinskaya V.S., Kotova N.P. Experimental Studies of Ta_2O_5 and Columbite-Tantalite Solubility in Fluoride Solutions from 300 to 550 °C and 50 to 100 MPa // J.Mineral and Petrol. 2010. V. 99. N. 3/4. P. 287–300

Novikov M.P., Gorbachev P.N. On the nature and quantitative content of water in aqueous phosphates of rare earths elements with the structure of rhabdofan *UDC 550.41 + 553.2*

Institute of Experimental Mineralogy RAS, Chernogolovka, Chernogolovka, Moscow district, Russia e-mail: novikovi@chgnet.ru

Abstract. In this work, we studied the physico-chemical properties of compounds of aqueous rare earth phosphates, the study of which is associated with the known difficulties of their very rare distribution in nature. Phosphates of the morphotropic series of synthetic analogues of rhabdofan are the main object of study. So far, for aqueous rare-earth phosphates with the rhabdophane structure, there are no consistent data on the form of water incorporation, its content, and, as a result, the generally accepted writing of the chemical formula. Based on the structural features of hydrated phosphates of the cerium subgroup, it is customary to consider the zeolite type of water for compounds with a hexagonal structure (Mooney R.C.L.J., 1950). Therefore, in accordance with the structure, the content of the latter should be 1.5 H_2O molecules per unit cell, or 0.5 mol per formula unit. However, according to many researchers, the amount of water of hydration for phosphates of this type is attributed to the most varied, from 1.5 to n H_2O mol (Ulyanov, Kazakova, 1963; Tananaev, Vasilyeva, 1963; Kozlova, 2020; A. Shelyug, 2018).
The reason for such large discrepancies in the H_2O contents, as well as the nature of its occurrence, lies, according to our data, in different degrees of crystallinity of synthetic samples. Considering the latter, the degree of crystallinity of synthetic samples was studied depending on various experimental conditions: pH (0.5–6)), concentration of components and water content in the obtained samples).

Keywords: kularite; huttonite; solubility; deposit; rare earths; sample; mineral.

Experimental technique

To obtain aqueous lanthanum phosphate, a hydrochemical method was used based on the precipitation reaction from a $LaCl_3$ solution diluted with phosphoric acid. Precipitation was carried out by a continuous method, by adding H_3PO_4 solution at a rate of 1-3 ml/min to a $LaCl_3$ solution in compliance with stoichiometry with continuous automatic stirring at a speed of 30 rpm for 24 hours, followed by exposure for 72 hours in the mother liquor. The precipitate that formed was separated by tecantation, washed with H_2O until it disappeared in a Cl^- solution, and dried to constant weight at 110°C.

The study of the synthesis products was carried out by various methods of quantitative analysis, as well as using an electron microscope. Ph was measured with an Ecotest-120 PH meter. The samples were samples of microcrystals in the form of folded leaflets collected in aggregates. The average particle size was about 1 μm.

Results and discussion

X-ray studies of the synthesis products indicate that with an increase in the pH value, the quality of the diffraction patterns deteriorates, up to the disappearance of the reflection altogether, i.e. before the transition of the samples to the X-ray morphic state (Fig. 1). An increase in the concentration of the reacting components (P and La) also acts in the same direction, with all other conditions of the experiments being constant.

A total of 50 samples of various degrees of crystallinity were synthesized. The most representative analyzes of the samples are presented in table. 1. As evidenced by the results of the analysis, the amount of water in the studied samples on the example of aqueous lanthanum phosphate is inversely related to the average particle size. The smaller the particle size, the greater the total content of H_2O in the samples. The latter circumstance obviously affects the nature of its isolation. To elucidate the reasons for this phenomenon, thermographic analyzes and various types of quantitative analysis, including the method of powder diffractometry, were carried out.

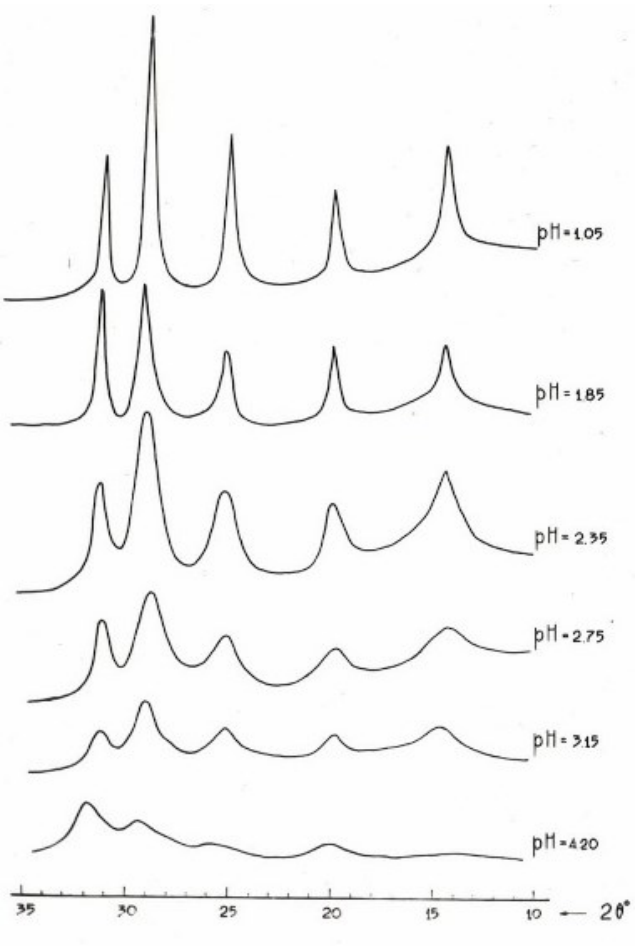

Fig. 1. Dependence of the degree of crystallinity of samples of aqueous La phosphate on the pH of the solution at 25°C according to powder diffraction data.

Table. 1. Results of chemical analysis of aqueous lanthanum phosphate varying degrees of dispersion**.**

№	Average particle size, microns	P_2O_5, wt.%	La_2O_3, wt.%	H_2O wt.%	Total
1*	≈1	29.62	66.50	3.79	99.91
2	≈1	29.24	66.90	3.81	99.95
3	≈1	29.32	66.92	3.74	99.97
4*	< 0.1	26.71	57.74	14.90	99.35
5	< 0.1	27.33	60.75	11.68	99.76
6	< 0.1	26.98	60.55	12.34	99.87

*) H_2O analysis was performed chromatographically on a CHN-1 analyzer at the IEM RAS. Without an asterisk - other methods of quantitative analysis (photoelectrocalometry, microprobe analysis).

A detailed thermographic analysis (Fig. 2) of dehydration clearly indicates the zeolite nature of water, the content of which, according to the structure of the mineral, is 1.5 molecules per 1 elementary cell or 0.5 mol in terms of one formula unit. Therefore, the chemical formula for the morphotropic series of synthetic analogs of rhabdofan is more correctly written as $LnPO_4 \cdot 0.5H_2O$, i.e. taking into account only zeolite water.

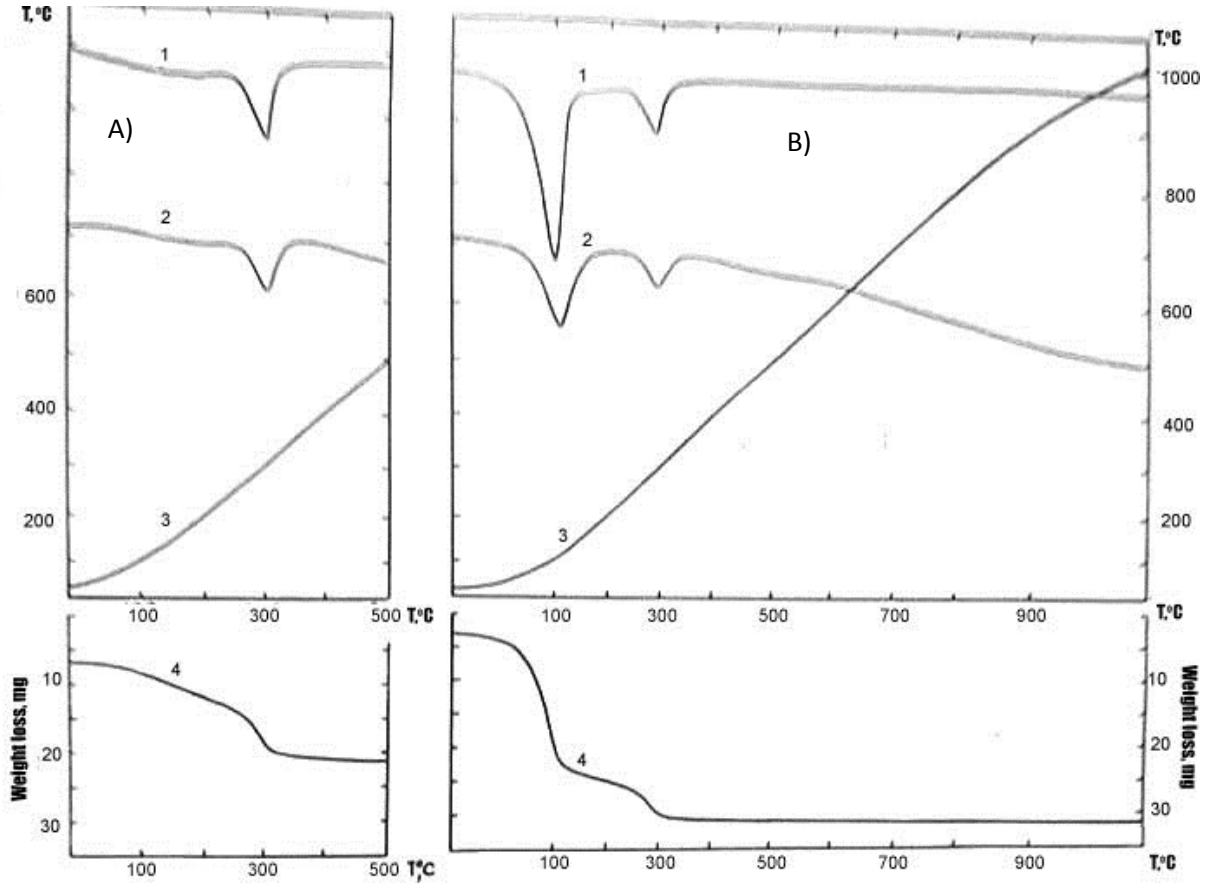

Fig. 2. Data from thermographic analysis of aqueous lanthanum phosphate. A - the initial record of the sample, previously calcined at 110ºC to constant weight; B - record after sample rehydration.

Conclusions

Thus, it was found that with an increase in the pH value and an increase in the concentration of the reacting components (P and La), the particle size decreases to the formation of X-ray precipitates. Therefore, the total amount of water in the samples is due to the non-crystallization of the samples, i.e. their amorphous state. As a result of the research, it was also found that the water in the samples is zeolite in nature and the chemical formula for rhabdofan and its synthetic analogues should be correctly written as $LnPO_4 \cdot 0.5H_2O$, which is consistent with the structure of the mineral.

References

Kozlova T.O. Synthesis, structure and physical and chemical properties of cerium (IV) orthophosphates: Dissertation for the competition. uch. Ph.D. - M., 2020 - S. 46-52.

Tananaev I.V., Vasilyeva V.P. On lanthanum phosphates // Journal of Inorganic Chemistry - 1963. - V.8. - S. 1070-1075.

Ulyanov A.I., Kazakova T.I. Synthesis and study of the properties of intermediate and basic ceroorthophosphates // Izvestiya AN SSSR, ser. chem. - 1963. - No. 3. – S. 393-397.

Mooney R.C.L.J. X-ray diffraction study of cerous phosphate and related crystals. I. Hexagonal modification // J.Acta Crystallogr. – 1950, №3. – P. 337-340.

A. Shelyug, A. Mesbah, S.Szenknect, N. Clavier, N. Dacheux and A. Navrotsk. Thermodynamics and Stability of Rhabdophanes, Hydrated Rare Earth Phosphates $REPO_4 \cdot nH_2O$. https://www.frontiersin.org/articles/10.3389/fchem.2018.00604/full2018. doi: 10.3389/fchem.2018.00604.

Redkin A.F., Kotova N.P. Study of romeite solubility in NaF solutions at 800 °C, 200 MPa and Cu_2O-CuO buffer.

Korzhinskii Institute of Experimental Mineralogy RAS
redkin@iem.ac.ru, kotova@iem.ac.ru

Abstract. Experimental data on the solubility of $(CaNa)Sb_2O_6F$ romeite in association with fluorite CaF_2 in NaF solutions in the concentration range from 1 to 8 mol·kg^{-1} H_2O at $f(O_2)$ given by the Cu_2O-CuO buffer have been obtained. Data from ICP and XRD analyzes indicate an increase in the solubility of romeite with increasing NaF concentration. It has been established that the dissolution of romeite occurs as a result of the removal of Sb^{5+} from structural positions, resulting in the formation of skeletal forms of fluorite. No new Sb-containing phases were found in the solid products of the experiments, according to XRD and SEM analyses.

Keywords: experiment, romeite, fluorite, skeletal forms of fluorite, solubility in the region of fluid immiscibility in the H_2O-NaF system, Sb^{5+} species

Romeite (Rom), (Ca, Na, Fe, $Mn)_2Sb_2^{5+}O_6(O,OH,F)$ is a rare mineral of the pyrochlore supergroup (Atencio et al., 2013). The composition of natural romeite is diverse and is determined by *T-p-f*(O_2) conditions and the environment (composition of the hydrothermal solution and host rocks) in which the crystals grew. According to (Brugger et al., 1997), fluorcalciоromeites could form under hypogenic conditions, i.e. in the depths of the Earth's crust, while hydro- or hydroxyl romeites were formed under supergene conditions (Kuzhuget, 2014; Eremin et al., 2018). According to few data, minerals containing antimony have low solubility at 25°C (Diemar et al., 2009). Experimental studies of the solubility of romeite under hypogene (or magmatic-hydrothermal) conditions have not been carried out. Of particular interest is the study in the field of fluid immiscibility of the NaF-H_2O system at 800°C, 200 MPa. These experimental studies are necessary to determine the composition and valence state of the predominant antimony complex particles in magmatic F-bearing hydrothermal solutions.

The experiments were carried out on a high-pressure hydrothermal apparatus at 800°C, P=200 MPa and Cu_2O-CuO oxygen buffer ($f(O_2)$ = 50.1 Pa). Run duration was 24 hours. In the run 15 mg of romeite (Rom) + 2 mg of fluorite (Flu) + 150 mg of H_2O + NaF (from 0 to 25 wt %) were injected into the Pt capsule. The oxygen buffer was prepared from a mixture of CuO and Cu_2O reagents in a ratio of 2:1. A mixture of CuO and Cu_2O in an amount of 50 mg was placed in a container, which was a 2 cm piece of a tube made of titanium alloy VT-8 from an armored thermocouple Ø = 5 mm, clamped at an angle of 120° or closed on both sides. The container used in the run was usually aged in several synthesis experiments.

The initial pure Rom $(CaNa)Sb_2O_6F$ was obtained by recrystallization of reagents mixture CaO+NaF+Sb_2O_5 in 1 *m*NaF at 800°C, 200 MPa, $f(O_2)$ = 50.1 Pa during the day. The sample/solution ratio was 3/1. Fluorite was used in the run, obtained from the reagent CaF_2 of special purity by recrystallization in 0.1 *m*HF at 500°C, 100 MPa for 2 weeks. The solutions after the run were washed out with approximately 30-fold volume of water (~5 ml) into volumetric polypropylene conical test tubes, the solid phases were precipitated by centrifugation (6000 rpm) for 2-3 min. Then, the solution aliquot was taken in an amount of 4 ml, in which the content of Na, Ca, and Sb was determined by the methods of inductively coupled plasma (ICP-AES, ICP-MS). The solid phases were examined on a Tescan Vega TS5130MM scanning electron microscope (SEM) and by X-ray powder diffraction (XRD) on a Bruker D2 Phaser digital X-ray diffractometer.

XRD analysis of buffer mixtures after the run at 800°C, 200 MPa showed that both CuO and Cu_2O oxide phases were retained in the mixtures.

In the solid products of experiments carried out in NaF solutions in the concentration range of 0 - 25 wt. % at $f(O_2)$ specified by the Cu_2 O-CuO buffer, according to XRD and SEM studies, the presence of two phases was noted: romeite and fluorite (Fig. 1). No new phases were found. Using the intensities of the <111> Flu and <311> Rom lines, the NaF concentration effect on the Flu/(Flu+Rom) ratio (in %) was calculated in the run products (Fig. 2). In the initial mixture, as in the experiment carried out in water, the Flu/(Flu+Rom) ratio was approximately 13%, while in the experiment with 25 wt. % NaF this ratio increased to 37 %.

In the products of the run carried out in water and 4.03 wt. % NaF, no significant changes in the crystalline phases are observed. Romeite after the run, as in the initial sample, is represented by small (<5 μm) octahedral crystals, and fluorite is represented by rounded grains. In solutions containing 10 - 25 wt. % NaF, a decrease in the content of Rom and the formation of skeletal forms of fluorite are observed (Fig. 3).

The solution after the runs, extracted from the Pt ampoules, was colorless. The results of the ICP analysis of solutions after the experiments are shown in Fig. 4. The analysis for the Sb content in dilute solutions performed at IPTM RAS (Chernogolovka) and at MSU, Faculty of Geology (Moscow) showed similar results.

In the runs carried out in NaF solutions in the concentration range of 4 - 25 wt. % and $f(O_2)$ specified by cuprite-tenorite buffer, there is a noticeable increase in the equilibrium content of Sb in the solution with increasing NaF concentration. The Rom solubility is significant and exceeds 10^{-2} $mol \cdot kg^{-1}$ H_2O.

Studies of incongruent romeite solubility with the formation of fluorite were carried out mainly in the region of fluid immiscibility of the NaF-H_2O system at 800°C, 200 MPa (Redkin et al., 2016).

Antimony in romeite (Sb-containing pyrochlore) is represented by Sb^{5+} ions in octahedral coordination. In the solution in the experiment mode, antimony should also be represented by Sb^{5+} particles, because in the case of Sb^{3+} particles, a decrease in $f(O_2)$ from 50 Pa (Cu_2O-CuO) to $10^{-3.47}$ Pa (Cu-Cu_2O) should have caused an increase in the Sb^{3+} concentration in the solution by more than 5 orders of magnitude, which was not observed in practice.

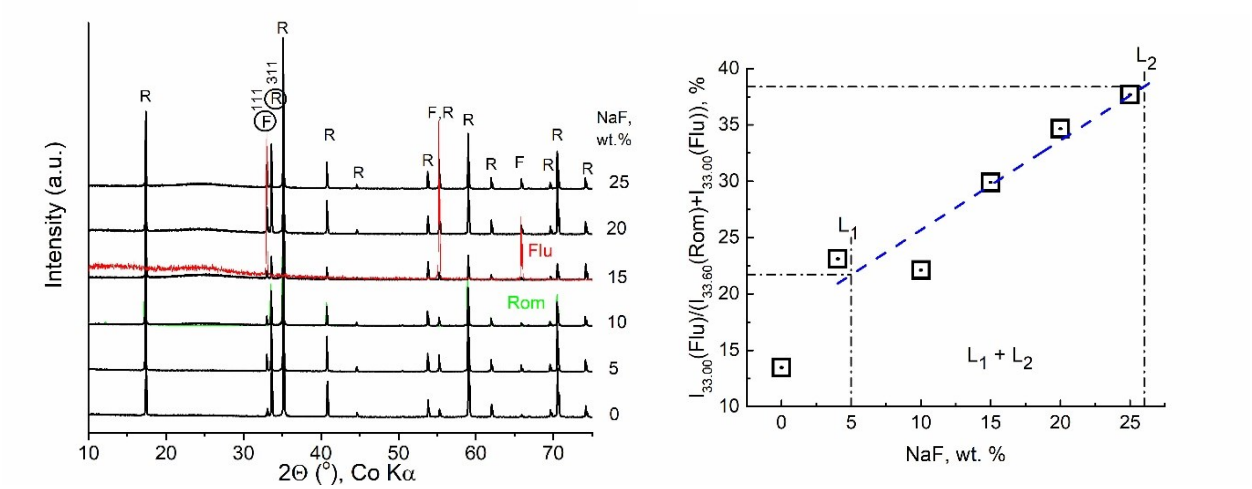

Fig.1. XRD of solid phases after experiments on Rom solubility in NaF solutions in the concentration range 0 to 25 wt. % at 800° C, 200 MPa and $f(O_2)= f(Cu_2O\text{-}CuO)$. Symbols: R - Rom, F - Flu.

Fig.2. Effect of NaF concentration on the relative intensity of the <111> Flu and <311> Rom lines in the run products on the solubility of a mixture of 15 mg Rom + 2 mg Flu at 800°C, 200 MPa and $f(O_2)= f(Cu_2O\text{-}CuO)$.

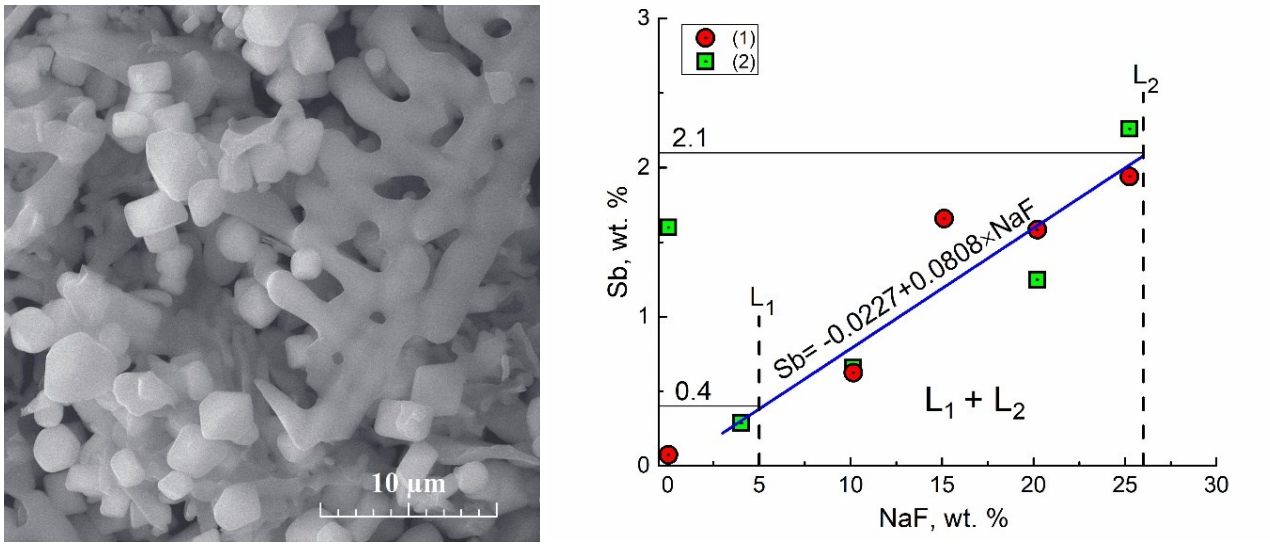

Fig.3. Micrograph (SEM) of solid phases after experiments at 800°C, 200 MPa in solutions containing 25 wt. % NaF, and $f(O_2)$ given by the Cu_2O-CuO buffer.

Fig.4. Dependence of C_{Sb}^{total} on C_{NaF}^{total}C in experiments on the incongruent Rom solubility at 800°C, 200 MPa. According to the results of ICP-MS analysis in laboratories: (1) - IPTM RAS; (2) – GEOL.MSU.

The data presented in fig. 4 characterize the apparent Sb concentrations, i.e. those values that are obtained as a result of mixing fluid phases L_1 (low density) and L_2 (high density). Assuming that the compositions of L_1 and L_2 remain constant, then the apparent concentration of antimony is determined by the leverage rule:

$$C_{Sb}^{total}(wt.\%) = X_{NaF}^{L1} \times C_{Sb}^{L1} + X_{NaF}^{L2} \times C_{Sb}^{L2} \quad (1)$$

where C is mass concentration of antimony (total), in the L_1 and L_2 fluid phases; X is the mass fraction of NaF, respectively, in the L_1 and L_2 fluid phases: . $X_{NaF}^{L1} + X_{NaF}^{L2} = 1$. Replacing the mole fractions of NaF of the L_1 and L_2 phases on the concentrations and, after some transformations, we obtain a linear dependence of the apparent antimony concentration on the total concentration of NaF:

$$C_{Sb}^{total}(wt.\%) = A \times C_{NaF}^{total} \times (C_{Sb}^{L1} - C_{Sb}^{L2}) + B \times (C_{Sb}^{L1} - C_{Sb}^{L2}) + C_{Sb}^{L2} \quad (2),$$

where $C_{NaF}^{total} = C_{NaF}^{L1} + C_{NaF}^{L2}$, $A = 1/(C_{NaF}^{L2} - C_{NaF}^{L1})$, $B = C_{NaF}^{L2}/(C_{NaF}^{L2} - C_{NaF}^{L1})$.

In equation 2, the variable parameters are C_{NaF}^{total} и C_{Sb}^{total}, while all other quantities in the selected water-salt system depend only on *T* and *P*. Having calculated the parameters of the linear equation according to the dependence of C_{Sb}^{total} on C_{NaF}^{total} at the values $C_{NaF}^{L1} = 5\ wt.\%$ and $C_{NaF}^{L2} = 26\ wt.\%$ (Redkin et al., 2016), antimony concentrations in the L_1 and L_2 phases were determined: $C_{Sb}^{L1} = 0.4\ wt.\%$ and $C_{Sb}^{L2} = 2.1\ wt.\%$ (Fig. 4).

Taking into account that the solubility of romeite in the studied solutions is significant, it can be assumed that dissolved antimony could affect the boundaries of fluid immiscibility in the NaF–H_2 O system. Because the concentration of antimony in a solution containing 4 wt. % NaF, corresponds to a linear approximation of C_{Sb}^{total} on C_{NaF}^{total}, we can conclude that the dissolved antimony led to the expansion of fluid immiscibility boundaries, and this, in turn, led to a decrease in C_{Sb}^{L1} and an increase in C_{Sb}^{L2}.

It should be noted that, in contrast to microlite (Redkin et al., 2016) and pyrochlore (Redkin et al., 2022), in which Ta and Nb concentrations decreased in the region of fluid immiscibility, the romeite solubility (the equilibrium content of Sb), on the contrary, increased with an increase in the total concentration of NaF. This behavior of these elements is associated with the composition of the predominant complexes. Upon dissolution of romeite, a significant amount of NaOH is formed in the L_1 fluid phase, which should be dominated by neutral Sb^{5+} complexes derived from SbO_2^+ or $H_3SbO_4^0$ (Filella and May, 2003; Herath at al., 2017). At 800°C, 200 MPa, such a particle could be SbO_2F^0. In the L_2 fluid phase, on the contrary, the main contribution is made by $NaSb(OH)_6^0$ particles derived from $Sb(OH)_6^-$, (or from $H_2SbO_4^-$) having octahedral coordination (Baes, Mesmer, 1976). Taking into account that the neutral hydroxocomplexes $H_3SbO_4^0$ or $Sb(OH)_5^0$ are stable in acid solutions, their share in the total Sb^{5+} content can be insignificant.

Conclusions. The solubility of romeite $(CaNa)Sb_2O_6F$ in the NaF-H_2O *P-Q* type system was experimentally studied in a wide range of sodium fluoride concentrations (from 0 to 25 wt. % NaF) at 800°C, *p*=200 MPa. It is shown that Sb-containing pyrochlore (Rom) at 800°C, 200 MPa is stable only in an oxidizing environment (Cu_2O-CuO buffer, $f(O_2)$ = 50 Pa). In fluoride solutions, romeite, which is in equilibrium with fluorite, has a significant solubility (*m* Sb), which increases in the region of fluid immiscibility with an increase in the total concentration of sodium fluoride and in the range of NaF concentrations from 1 (4 wt. % NaF) to 8 mol·kg^{-1} H_2O (25 wt.% NaF) is in the range $2\cdot10^{-2}$ – $2\cdot10^{-1}$ mol·kg^{-1} H_2O. For the first time, the solubility method was used to estimate the of antimony concentrations in the L_1 and L_2 phases in the region of fluid immiscibility in the NaF-H_2O system at 800°C, P=200 MPa and $f(O_2)$ specified by the Cu_2O-CuO buffer. It has been established that skeletal forms of fluorite are formed during of the romeite dissolution.

It can be assumed that the main contribution to the romeite solubility in the L_1 fluid phase is made by particles of SbO_2F^0 and $Sb(OH)_5^0$, and in the L_2 phase containing 26 wt. % NaF, the predominant particle is $NaSb(OH)_6^0$.

The work was carried out on the topic: FMUF-2022-0003 and with the financial support of the Russian Foundation for Basic Research grant 20-05–00307a.

The authors are grateful to Drozhzhina N.A. (IEM RAS) for X-ray analysis of solid experimental products, Ph.D. Karandashev V.K. (IPTM RAS) and d.g.-m.s. Bychkov A.Yu. (Moscow State University) for ICP analysis of solutions after experiments.

References

1. Eremin O.V., Yurgenson G.A., Solodukhina M.A., Epova E.S. Hypergene Antimony and Bismuth Minerals: Methods for Estimating Their Standard Gibbs Potentials // In: Mineralogy of technogenesis-2018. RAS. Ural branch. 2018. P. 103-131.
2. Kuzhuget R.V. Gold-telluride mineralization of the Aldan-Maadyr ore cluster (Western Tuva): mineralogical and geochemical features of ores and conditions for their formation // Dis. cand. g.-min. sc. Kyzyl. 2018. 152 p.
3. Redkin A.F., Kotova N.P., and Shapovalov Yu.B. Liquid immiscibility in the system NaF-H2O and microlite solubility at 800°C // Doklady Earth Sciences. 2016. V. 469. N.2. P. 722–727.
4. Redkin A.F., Kotova N.P., and Shapovalov Yu.B. Pyrochlore Solubility in NaF Solutions at 800°C and P = 170–230 MPa // Doklady Earth Sciences. 2022. V. 507. N. 1. P. 887-900.
5. Atencio D., Ciriotti M.E., and Andrade M.B. Fluorcalcioroméite, (Ca,Na)2Sb25+(O,OH)6F, a new roméite-group mineral from Starlera mine, Ferrera,

Grischun, Switzerland: description and crystal structure // Mineral. Mag. 2013. V. 77. P. 467-473.
6. Baes C.F.Jr., Mesmer R.E. The Hydrolysis of Cations. John Wiley-Interscience: New York, NY, 1976. P. 370–375. 489 P. ISBN: 0471039853, 9780471039853
7. Brugger J., Gieré R., Graeser S., and Melsser N. The crystal chemistry of romeite // Contrib. Mineral. Petrol. 1997. V. 127. P. 136–146.
8. Diemar G.A., Filella M., Leverett P., and Williams P.A. Dispersion of antimony from oxidizing ore deposits // Pure Appl. Chem. 2009. V. 81(9). P. 1547–1553.
9. Filella M., May P.M. Computer simulation of the low-molecular-weight inorganic species distribution of antimony(III) and antimony(V) in natural waters // Geochim. Cosmochim. Acta. 2003. V. 67(21). P. 4013–4031.
10. Herath I., Vithanage M., and Bundschuh J. Antimony as a global dilemma: Geochemistry, mobility, fate and transport // Environ. Pollut. 2017. V. 223. P. 545–559.

Rusak A.A.[1], Shchekina T.I.[2] Mineral parageneses of cryolite-containing rare-metal deposits *UDC 553.08, 552.13*

[1]Vernadsky Institute of Geochemistry and analytical chemistry RAS (GEOKHI RAS), Russia, 119991, Moscow, st. Kosygina, 19, aleks7975@yandex.ru, [2]Lomonosov Moscow State University, Department of Geology, Russia, 119991, Moscow, st. Leninskiye gory, 1, t-shchekina@mail.ru, 8 (495) 939-70-05.

Abstract. In this work, rare metal cryolite-containing granites from three deposits of Eastern Siberia were studied are Zashikhinsky, Katuginsky and Ulug-Tanzek. In each of these deposits there are leucocratic alkaline (K_2O+Na_2O~9 wt.%) lithium-containing granites with high contents of niobium, zirconium, rubidium, hafnium, to a lesser extent tantalum, as well as uranium, thorium and rare earth elements. A typical accompanying mineral of these granites is cryolite. When studying the corresponding rocks, it was found that cryolite most often forms nests or streaked-interspersed secretions of light brown or gray color. Cryolite is in paragenesis with potassium feldspar, acid plagioclase, lithium mica – polylithionite. Ore minerals are often crystallized together with cryolite: columbite, zircon, torite, gagarinite, galena, pyrite, etc. Similar parageneses of rock-forming and ore minerals were obtained in our experiments when studying a lithium-containing, fluorine- and water-saturated model granite system. Cryolite crystallizes from a salt melt, and together with it, fluorides of rare earth elements, torite, zircon and others are formed. These data confirm that cryolite can serve as a reference mineral of rare-metal-rare-earth mineralization in lithium-containing fluorine-saturated rare-metal granites.

Keywords: cryolite; leucocratic granite; rare metals; rare earth elements; ore.

Introduction Cryolite-containing granites are rare–metal granites in which the rock-forming mineral is cryolite. Cryolite is also formed in pegmatites from residual solutions enriched with fluorine (Betekhtin, 1950). About 20 ore occurrences of cryolite associated with rare-metal granites are known in the world. Cryolite deposits are very rare, the first large industrial deposit was discovered in Western Greenland (Ivigtut), now it has been developed. At this deposit, cryolite forms large crystalline masses within the granite massif and associates with cassiterite, zircon, magnetite, ilmenite, columbite, siderite, sulfides, etc.

The purpose and objectives of the work

The aim of the work was to study the paragenesis of minerals of lithium-fluorine-containing rare-metal leucocratic granites containing cryolite. The rocks of three rare-metal deposits of Eastern Siberia were selected as objects of research are Ulug-Tanzek, Zashikhinskoye and Katuginskoye.

In connection with this goal, the following tasks were solved are: a) to select representative samples of rare-metal granite rocks containing ore minerals and cryolite; b) to study samples in sections on an optical microscope and determine the composition of minerals on a microanalyzer; c) to identify mineral parageneses of cryolite-containing rare-metal granites at three deposits are Ulug-Tanzek, Zashikhinskoye and Katuginskoye; d) to compare the available experimental data on a model granite the fluorine-containing Si-Al-Na-K-Li-F-O-H system with the obtained natural data.

Methodology

To study the chemical composition of rocks, transparently polished plates were made at the Lomonosov Moscow State University and the Vernadsky GEOKHI of the Russian Academy of Sciences. Studies on rocks from the Zashikhinsky deposit were carried out on a scanning electron microscope Jeol JSM-6480LV (Jeol, Japan) with an energy-dispersion spectrometer Oxford X-maxN (Oxford Instrument Ltd., Great Britain), acquired at the expense of the Moscow University Development Program, in the laboratory of Local research methods of the Department of Petrology and Volcanology of the Geological Faculty of Moscow State University. Electronic images of the sample structure, phase morphology, and phase relations were obtained in the reflected electron (BSE) mode. Samples from the Katuginsky and Ulug-Tanzek deposits were studied using an Olympus BX 51 optical microscope at GEOKHI RAS and a Leica polarization microscope (Leica Microsystems, Germany) at the Department of Petrology and Volcanology of the Geological Faculty of Lomonosov Moscow State University.

The main objects of the study were three deposits of Eastern Siberia are Zashikhinskoye, Katuginskoye and Ulug-Tanzek (Fig. 1).

All the studied deposits are similar to each other in terms of mineral paragenesis. Firstly, these are

tantalum-niobium deposits confined to leucocratic alkaline (K_2O+Na_2O~9 wt. %) granites, the typical accompanying mineral of which is cryolite. They are characterized by high contents of zirconium, rubidium, lithium, rare earth elements, uranium and thorium. Secondly, these are polymetal deposits containing complex ores, they are saturated, in addition to rare and ore metals, with copper, iron, aluminum.

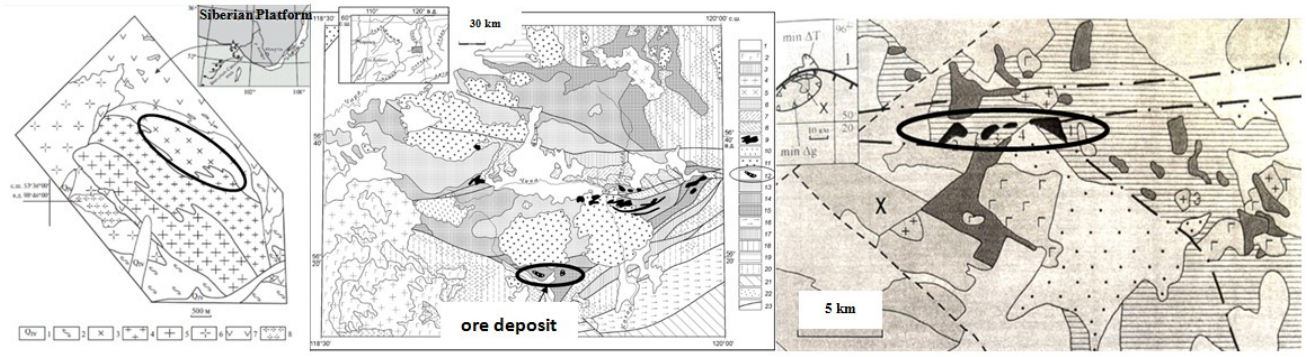

Fig. 1. Schematic geological maps are a) the Zashikhinsky massif (Alymova, Vladykin, 2018); b) the Udokan subzone of the Kodaro-Udokan trough (the area of rare-metal granites of the Katuginsky complex is highlighted) (Sklyarov et al., 2016); c) the Ulug-Tanzek ore node (Beskin, 2014). The areas where rare metal cryolite-containing granites were found are highlighted with black ovals.

Below is the mineral composition of leucocratic cryolite-containing granites for the three studied deposits of Eastern Siberia, compiled on the basis of studying the collections of field materials of T.N. Shuriga (provided by the VIMS Mineralogical Museum) and printed works of V.V. Arkhangelskaya and T.N. Shuriga in the 80s of the XX century. According to these data, a list of mineral parageneses by deposits was compiled are a) Ulug-Tanzek are quartz (pea-shaped), microcline, amazonite, albite, muscovite, polylithionite, zinnvaldite, biotite (Li-biotite), ribekite, arfvedsonite, cryolite, thomsenolite, pyrochlore, columbite, cryophyllite, beryl, fluorite, zircon, malacon, iron hydroxides (red-brown oxides), torite (ferritorite), gearksutite, xenotime, gagarinite, galena, molybdenum, Ce-britolite, Ce-rincolite, sphene, aegirine, orthite, ilmenite, galloisite, topaz, phenakite, fergusonite, euxenite, gadolinite, monazite, etc., as well as carbonates; b) Zashikhinskoe are quartz (pea-shaped), microcline, albite (sugar-like), protolithionite, Li-biotite, columbite (ferrocolumbite), zircon, sphalerite, pyrochlore, polylithionite, cryolite, fluorite, ribekite, iron hydroxides, Mn-oxides, etc; c) Katuginskoe are quartz, microcline (often porphyritic secretions), albite, amphibole, aegirine, cryolite (blue, pale green, (dark) gray, light brown), gagarinite, biotite, arfvedsonite, zircon, malacon, pyrochlore, ribekite, lepidomelan, fergusonite, columbite, thomsenolite, prosopite, ralstonite (aggregates of crystals on gagarinite), pakhnolite, gearksutite, ittrofluorite, ilmenite, gadolinite, etc.

When studying the parageneses of natural samples of the Zashikhinsky deposit provided by A.Y. Bychkov, we identified the following patterns. The main rock-forming minerals of granites were quartz, albite, feldspar, polylithionite (lithium mica), fluorite and ore minerals are zircon, columbite, xenotime, thorianite, torite and titanium-niobium phase (Fig. 2). Iron oxides are found as secondary minerals. Cryolite was not detected in the studied samples.

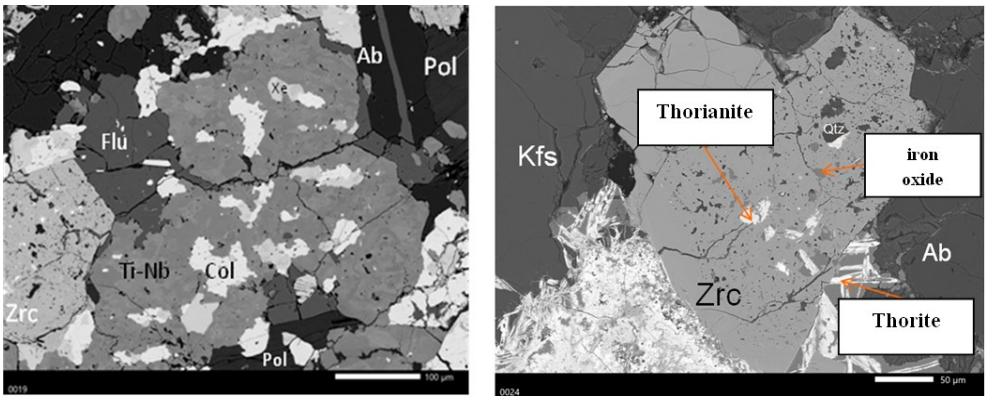

Fig. 2. Mineral paragenesis of the Zashikhinsky deposit (electron microscopic images in BSE mode). Symbols: Ab – albite, Pol – polylithionite, Flu – fluorite, Zrc – zircon, Col – columbite, Ti-Nb – titanium-niobium phase, Xe – xenotime.

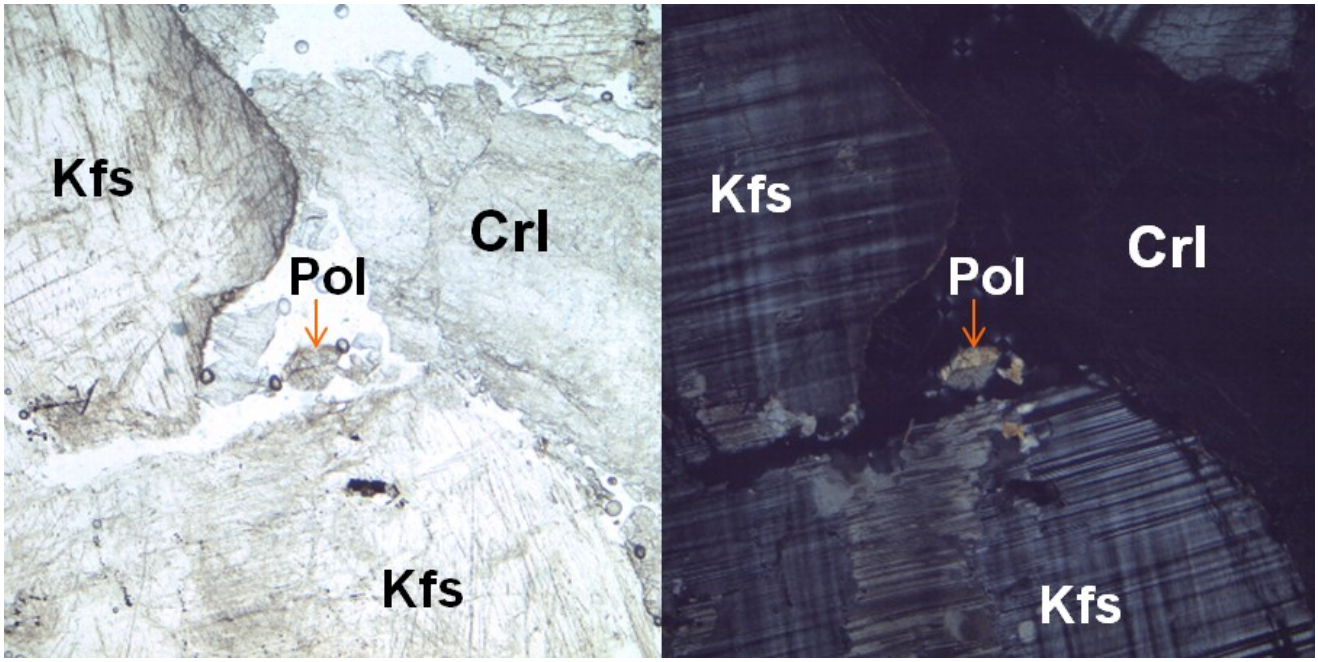

Fig. 3. Cryolite (Crl) crystallizes in interstitions of potassium feldspar (Kfs) and Li-mica– polylithionite (Pol) (photo of the slot on an optical microscope).

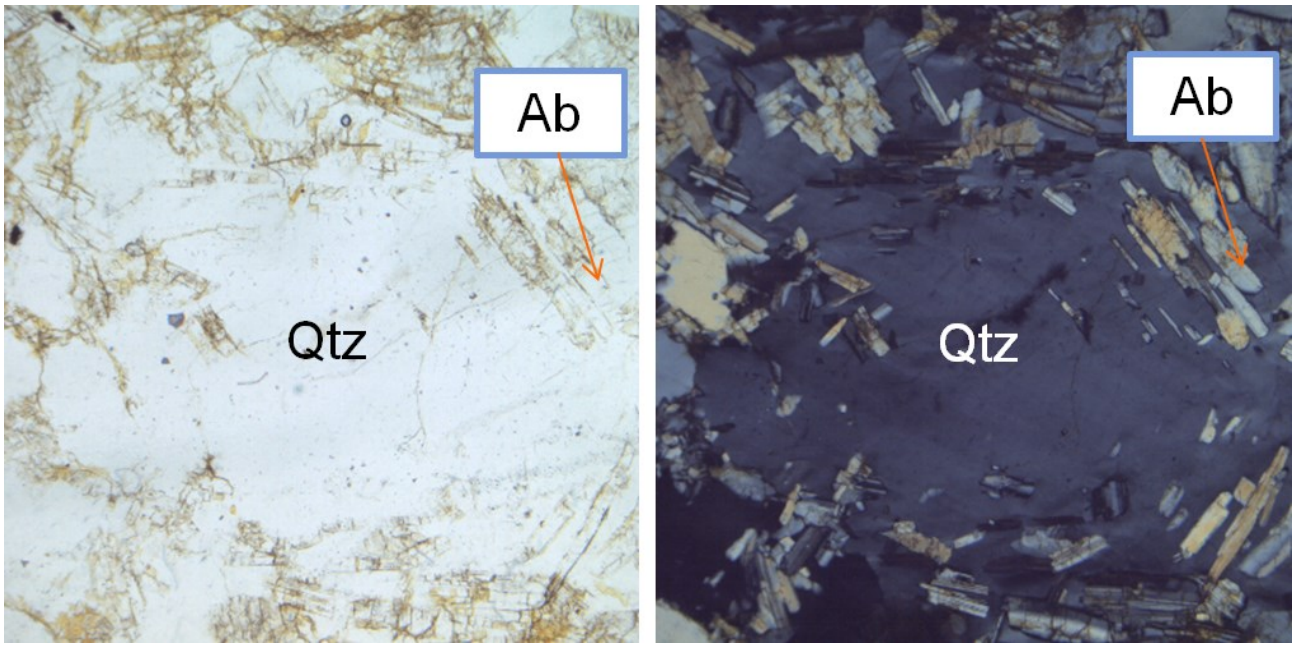

Fig. 4. The "snowball" structure formed by albite (Ab) crystals inside a quartz crystal (Qtz) (photo of the slot on an optical microscope).

In rare-metal cryolite-containing granites of the Katuginsky deposit, the main rock-forming minerals were're quartz, potassium feldspar, plagioclase, cryolite (Fig. 3), thomsenolite (secondary mineral according to cryolite), alkaline amphibole, polylithionite; from ore is zircon. Cryolite crystallizes frequently between potassium feldspar and mica.

The samples of cryolite-containing granites of Ulug-Tanzek do not differ much in the parageneses of the Katuginsky deposit, but a typical structure of a "snowball" in a quartz crystal by albite crystals was found in them (Fig. 4).

Similar parageneses of rock-forming and ore minerals were obtained in our experiments (Gramenitsky et al., 2005; Shchekina et al., 2020, 2021) when studying a lithium-containing, fluorine- and water-saturated model granite system. Cryolite (Crl) crystallizes at 700°C and 1 kbar from a salt melt formed in the system due to the liquid immiscibility of silicate L and salt LF melts (Fig. 5). It is surrounded by a rim of residual melt Lres enriched with fluorides of rare earth elements.

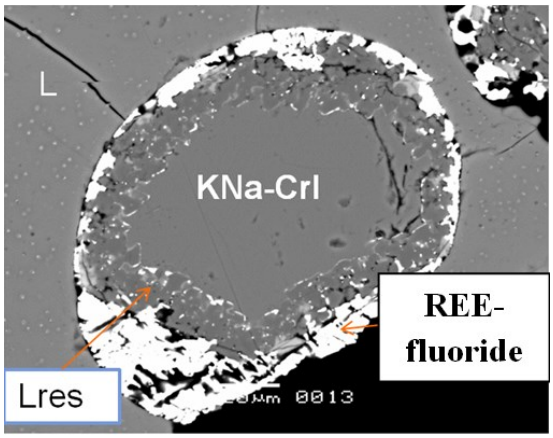

Fig. 5. A single crystal of KNa-Crl is surrounded by a sufficient Lres melt accumulating all REE at 700°C and 1 kbar (experimental study). Electron microscopic image in BSE mode.

Conclusions. All the studied rocks of the three deposits of Eastern Siberia, in general, are similar to each other in the paragenesis of minerals. They are represented by leucocratic alkaline fluoride-lithium-containing granites with high contents of niobium, zirconium, tantalum, thorium and REE. All rocks contain cryolite salt (Na_3AlF_6) and Li mica. The ability of salt melts to concentrate Li, REE and a number of other elements, discovered in experiments in a fluorine- and lithium-containing granite system, explains the fact that all cryolite-containing granites are accompanied by rare-metal-rare-earth mineralization. Rare earth elements are part of oxides, silicates, phosphates, carbonates and fluorides along with rare elements (Ta, Nb, Zr, Hf) and actinides (U, Th) and also form their own minerals such as gagarinite ($NaCaYF_6$), tveitite ($(Y,Na)_6(Ca,Na,Y)_{12}(Ca,Na)F_{42}$), fluocerite ($(La,Ce)F_3$), costinite ($NaYF_4$), etc. When searching for rare-earth elements, cryolite can serve as a reference mineral of rare-metal-rare-earth mineralization characteristic of alkaline rare-metal granites.

The work was carried out with the support of the state assignment of the GEOKHI RAS, on the state budget topic "Modes of petrogenesis of the Earth's internal geospheres" of the Geological Faculty of Lomonosov Moscow State University and with the financial support of the RFBR grant (project № 16-05-0089).

The authors express gratitude to A.Y. Bychkov for the stone material provided from the Zashikhinsky deposit.

References:

Alymova N.V., Vladykin N.V. Ore content of rare-metal granites of the Zashikhinsky massif (Irkutsk region) and concentrator minerals Ta, Nb, Th, Zr, TR // News of Irkutsk State University. Earth Science Series. 2018. Vol. 25. pp. 15-29 [in Russian].

Beskin S.M. Geology and indicator geochemistry of tantalum-niobium deposits of Russia (rare-metal granites) / Beskin S.M. — M.: Scientific World, 2014. — 111 p.: il. [in Russian].

Betekhtin A.G. Mineralogy — M.: State Publishing House of Geological Literature, 1950. — 956 p. [in Russian].

Gramenitsky E.N., Shchekina T.I., Devyatova V.N. Phase relations in fluorine-containing granite and nepheline-syenite systems and the distribution of elements between phases. M.: GEOS. 2005. 186 p. [in Russian].

Sklyarov E.V., Gladkochub D.P., Kotov A.B., Starikova A.E., Sharygin V.V., Velikoslavinsky S.D., Larin A.M., Mazukabzov A.M., Tolmacheva E.V., Khromova E.A. Genesis of the Katuginsky rare metal deposit: magmatism against metasomatosis // Pacific Geology, 2016, vol. 35, № 3, pp. 9-22. [in Russian].

Shchekina T.I., Rusak A.A., Alferyeva Ya.O., Gramenitsky E.N., Kotelnikov A.R., Zinovieva N.G., Bychkov A.Yu., Bychkova Ya.V., Khvostikov V.A. Distribution of REE, Y, Sc and Li between aluminosilicate and aluminofluoride melts in a model granite system depending on pressure and water content. Geochemistry 65, 4 (2020), 343-361. [in Russian].

Shchekina T.I., Rusak A.A., Alferyeva Ya.O., Gramenitsky E.N., Khvostikov V.A., Kotelnikov A.R., Bychkov A.Yu., Zinovieva N.G. Lithium behavior in the liquidus part of a high-fluoride granite system at a pressure from 10 to 50 MPa. Bulletin of the Moscow University. Series 4: Geology, 3 (2021), 76-88. [in Russian].

Balabin A.I. Linear polymerization of water and ions as the mechanism behind liquid immiscibility phenomena in water–salt systems *UDC* 544.344.2

Institute of Experimental Mineralogy RAS, Chernogolovka
balabinmtv@yahoo.com

Abstract. A number of binary and ternary water–salt systems display miscibility gaps within the liquid or supercritical fluid solution regions characterized by the existence of a lower critical solution temperature (LCST). In these systems, complete miscibility is observed within a wide composition range at temperatures below the LCST and, as the T_{LCST} is exceeded, a miscibility gap emerges ever widening with further increase in the temperature. Water–salt systems with LCST display a common set of features indicative of a common molecular mechanism responsible for immiscibility. Remarkably, these same features are characteristic of polymer solutions in low molecular weight solvents. In polymer solutions, immiscibility takes place when polymer molecules undergo the conformational coil-to-globule transition. By analogy, immiscibility phenomena in water–salt systems are explained in the present article as a consequence of linear polymers present in the solution and undergoing a coil-to-globule transition. Analysis of phase diagrams and the published thermochemical data leads to the conclusion that

these polymers are composed of water molecules as well as ions. Occasionally, fragments of such polymeric chains are found incorporated into the crystal structure of hydrated salts, as is the case with β-$Na_2HPO_4 \cdot 12H_2O$, a hydrated salt that contains a polyanion $[(HPO_4)_8(H_2O)_{12}]^{16-}$ organized around a chain comprised by 12 water molecules.

Keywords: water–salt systems, equilibrium liquid–liquid, linearly polymerized water, coil-to-globule transition.

Introduction. Immiscibility regions in most solutions are characterized with an upper critical solution temperature (UCST). In these familiar systems, the miscibility is complete at $T > T_{UCST}$, and at $T = T_{UCST}$ a miscibility gap emerges in which two solutions of different composition coexist in equilibrium, the contrast of coexisting compositions ever-increasing as the temperature continues to decrease. Aqueous solutions of a number of electrolytes display a diametrically opposed, counterintuitive behavior. These water-salt systems are characterized with a low critical solution temperature (LCST). The solution is homogeneous in such systems at $T < T_{LCST}$ within a wide composition range spanning from pure water to the compositions saturated with some crystallized salt, but a miscibility gap emerges as the temperature rises to T_{LCST}, and the gap is widening continually as the temperature keeps rising, e.g., see the phase diagram of the binary system Na_2HPO_4–H_2O, Fig 1.

In the present work a survey of binary and triple water-salt systems with LCST is undertaken with the aim of elucidating the mechanism of liquid immiscibility in them. Shown below are conclusions reached based on comparative analysis of the data available. First, it is shown, based on the temperature intervals spanned by coexisting liquids in various systems, that there is no connection between the phase separation into two liquids and the critical phenomena associated with the gas – liquid transition in water. Next, physicochemical features of water-salt systems with LCST are discussed to some detail. Taken together, these bear striking similarities with features characteristic of polymer solutions in low molecular weight solvents. In polymer solutions, liquid immiscibility takes place when the polymer molecules undergo a coil-to-globule transition. In view of this, a hypothesis is put forth interpreting liquid immiscibility in aqueous electrolyte solutions as a manifestation of polymerization. Phase separation into two liquids occurs when these polymers experience a coil-to-globule transition. An attempt to elucidate the nature of these polymers is taken in the next part of the article. On the one hand, particulars of phase diagrams in the light of analogies with polymer solutions suggest that these are to be polymerized ions – polyanions or polycations. On the other, correlations with Hofmeister series and a published appraisal of thermodynamics of ion hydration imply that these polymers contain water molecules. The polymers are, thus, made up of ions and water molecules. The final section of the article presents the outcome of a search through crystal structures of hydrated salts carried out in the course of the present work with the purpose of finding polymerized ions. If a polymerized ions present in an aqueous solution are captured during the crystallization and embedded into the crystal network, perhaps fragmented and shaped liked globules, their appearance in the structure would validate the proposed attribution of liquid immiscibility to polymerization phenomena in aqueous electrolyte solutions. An example of such an ion comprising a chain of water molecules decorated with groups $[HPO_4^{2-}]$ is provided in that section thereby corroborating the proposed theory.

The liquid immiscibility in water – salt systems with LCST is not related to the gas – liquid critical phenomena. Historically, a few water – salt systems with LCST that were studied first all had their critical phase separation temperatures, T_{LCST}, within ± 100°C of the critical point of water (374°C). In view of this, many scientists assume that liquid immiscibility is somehow related to the gas – liquid transition in these systems, the solution with low salt concentrations being the supercritical fluid and the concentrated solution being either liquid water stabilized by an extra amount of salt dissolved in it or a molten salt with some amount of water dissolved in it. In light of experimental studies accumulated more recently, any connection between the two types of critical phenomena is ruled out by mere comparison of T_{LCST} values. The low critical solution temperatures published so far for binary and triple system span a wide temperature range: 32°C for the system Bu_4NF–NH_4F–H_2O, (Aladko, Dyadin, 1994); 222°C for $CdSO_4$–H_2O (Wan et al., 2017); 260°C for $MgSO_4$–H_2O (Wang et al. 2013); 286°C for UO_2SO_4–H_2O (Marshall, Gill, 1974); ~337°C for Li_2SO_4–H_2O (Urusova, Valyashko, 2014); 360°C for K_2HPO_4–H_2O (Marshall et al., 1981); ~375°C for $ZnSO_4$–H_2O (Urusova, Valyashko, 2019); ~460°C for K_2SO_4–KCl–H_2O (Urusova et al., 2007); ~760°C for NaF–H_2O (Redkin, Kotova, 2016). The known T_{LCST} values vary in the temperature range whose lower bound is circa 300°C below the critical temperature of water and the upper bound is about 300°C above it. Obviously, both phases, L_1 and L_2, comprise liquid water in the system Bu_4NF–NH_4F–H_2O at 32 through 70 °C, Fig 3, whereas the two phases L_1 and L_2 comprise subcritical fluid in the system NaF–H_2O at 800°C, Fig 4. Therefore, there is no relation between liquid – liquid phase separation in water – salt systems with LCST and the liquid – gas transition.

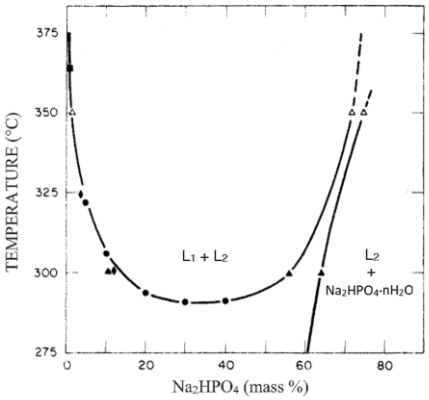

Fig. 1. Condensed system Na_2HPO_4–H_2O, 250–400 ^{0}C. L_1 and L_2 denote respectively, the dilute and concentrated liquid solutions. *Modified from* (Marshall, 1982).

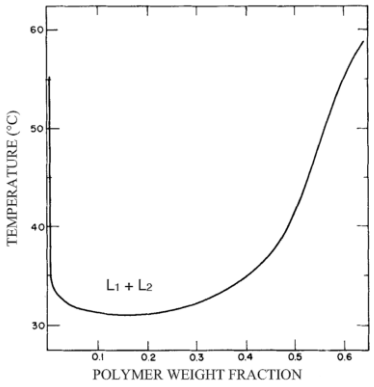

Fig. 2. Phase diagram of aqueous solutions of poly(N-isopropyl acrylamide). L_1 and L_2 denote respectively, the dilute and concentrated solutions. *After* (Heskins, Guillet, 1968).

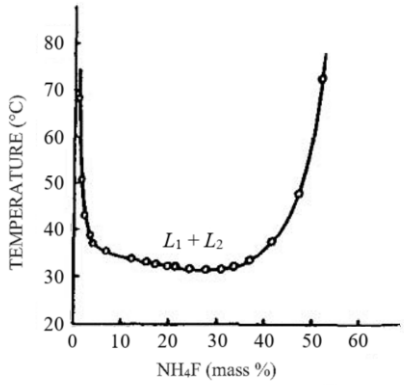

Fig. 3. The section (65 mass % Bu_4NF) for the liquid region in the system Bu_4NF–NH_4F–H_2O. *Modified from* (Aladko, Dyadin, 1994).

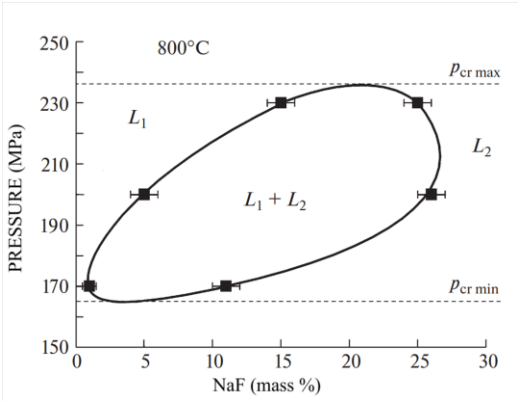

Fig. 4. The immiscibility field in the system NaF–H2O at 800 °C as delineated experimentally by (Redkin, Kotova 2016).

Characteristic features of water-salt systems with LCST. Binodal curves delimiting compositions of coexisting liquids in water-salt systems with LCST invariably display a shape resembling "a flat bottom with rounded edges" on the phase diagram. To put in other words, the binodal appears to have a near-zero curvature in the proximity of LCST, so that coexisting compositions diverge swiftly as soon as the temperature exceeds T_{LCST}, and on further increase in temperature a concentrated solution (nearing saturation with a crystalline salt hydrate) coexists with essentially pure water, Fig 1 and Fig 3.

Coexistence of water practically devoid of salt with a concentrated solution approaching saturation at temperatures significantly exceeding the T_{LCST} is a phenomenon observed for a number of phase diagrams of water-salt systems with LCST. As another manifestation of this same phenomenon, a solution with a relatively low salt content will separate into two distinct liquids at sufficiently high temperatures. This type of phase behaviour has also been observed, namely: turbidity in aqueous solution containing as little as 0.434 mass% K_2HPO_4 has been observed at 367°C in the system K_2HPO_4-H_2O by (Reimer, Vogel, 2016). In the system K_2SO_4–Na_2SO_4–H_2O, turbidity has been observed in a solution with total salt concentration as little as 0.1 mol/kg H_2O at 374°C by (Reimer, Vogel, 2013).

A positive volume effect of phase separation. Valyashko and Urusova have investigated phase relations for a number of binary and triple water-salt systems with LCST by constructing and analyzing P – V curves for various selected compositions. Measured in these experiments (carried out in Ravich vessel design) are changes in pressure accompanying small successive incremental volume enlargements of the system. According to the large body of data published by these authors, the appearance of the second liquid (i.e., formation of droplets of the concentrated solution via reduction of the amount of the first liquid—less concentrated solution) always takes place when the pressure in the system is diminished somewhat. According to Le Chatelier's principle, this means that the phase transformation is accompanied by an increase in molar volume.

A small endothermic effect of phase separation. Liquid immsicibility in dilute aqueous solutions of two salt mixtures, K_2SO_4-Na_2SO_4 and Na_2SO_4-Na_2HPO_4, have been investigated by (Reimer, Vogel, 2016) utilizing high pressure differential scanning calorimetry. In both systems the liquid-liquid phase separation is detected as a slight endothermic effect.

Abnormal sensitivity to pressure changes. Small changes in hydrostatic pressure typically affect the phase equilibria that involve gases, but phase boundaries of condensed matter respond to such changes with no or at most minor shifts. A notable exception to the rule is set by liquid – liquid equilibria in water-salt systems with LCST. In the latter systems boundaries of liquid – liquid regions are usually delineated by measuring the temperature, for a fixed composition, at which the emergence of the second liquid manifests itself as turbidity or cloud point (CP). The temperature T_{CP} has been investigated as a function of pressure for various compositions in two systems, UO_2SO_4–H_2O and $CdSO_4$–H_2O, by (Marshall, Gill, 1974; Wan et al., 2017). In both systems an increase in pressure facilitates mutual solubility of the two liquids so that T_{CP} increases with the rise in pressure with the gradient, $\frac{dT_{CP}}{dP}$, respectively, 0.075 °C/bar and 0.05 °C/bar – abnormally steep values so long as condensed matter physical chemistry is concerned.

Gelation. As mentioned above, a concentrated solution coexists in equilibrium with water containing tiny amounts of salt in the phase separation region of a wates-salt system with LCST if the temperature exceeds the T_{LCST} significantly. If quenched, these concentrated solutions turn into a gel (Marshall, 1975).

Similarities between aqueous electrolyte solutions with LCST and polymer solutions.

As was mentioned previously, liquid – liquid phase separation caused by an increase in temperature and thus characterized with a LCST is generally unusual. However, it is this type of phase behaviour that comprises a most distinctive feature of high polymer solutions (Paterson et al., 1967). Polymer solution experience phase separation into two or more distinct liquids when the polymer molecules undergo a conformational coil-to-globule transition.

Coil-to-globule transition is a collapse of a macromolecule from an expanded coil state to a compact globule state. Such a transformation has been observed in a plethora of polymer solutions of different nature: neutral polymers dissolved in water as well as in other low molecular weight solvents, and in ionic liquids. It was also observed for various charged polymers dissolved in water (strong cationic polyelectrolytes, such as poly(2-vinyl pyridine) and poly(methacryloyloxyethyl dimethyl benyl ammonium chloride), a weak cationic polyelectrolyte poly(vinylamine), polymerized anions, such as sodium polystyrene sulfonate and DNA).

Coil-to-globule transition in dissolved polymers invariably results in a phase separation of the solution into (at least) two immiscible liquids, and typically the corresponding miscibility gap on the phase diagram is characterized with a LCST, as is the case with the system Poly(N-isopropylacrylamide–water Fig 2 (though miscibility gaps with UCST and other more complicated types of phase diagrams have also been encountered). The shape of the binodal in the Fig. 2 is characteristic of polymer solution with LCST in such features as a near-zero curvature in the proximity of LCST and a wide temperature range within which a concentrated solution coexists with essentially pure solvent. Recall that these same features are displayed by phase diagrams of water – salt systems with LCST, Fig. 1 and Fig. 3.

Furthermore, the coil-to-globule transition is detected calorimetrically as a minor endothermic effect (Zhang et al., 2017; Crespy, Rossi, 2007) and this transformation proceeds with an increase in volume (Wolf, 1997), (Saeki *et al.*, 1973), in complete analogy with what was observed in the water – salt systems with LCST. Next, coil-to-globule transition in polymer solutions shows high sensitivity to changes in hydrostatic pressure, abnormal to equilibria involving condensed phases. Typically, the cloud point (turbidity temperature for a fixed composition) rises swiftly with an increase in pressure (Wolf, 1997), (Saeki *et al.*, 1973), once again in agreement with what is observes in water – salt systems with LCST. Finally, concentrated polymer solutions tend to form gels at low temperatures and this same phenomenon has also been observed in water–salt systems with LCST.

In view of the aforementioned similarities between polymer solutions and aqueous electrolyte solutions with LCST, one is temped to hypothesize that linear polymers are present in aqueous electrolyte solutions. These polymers undergo a coil-to-globule transition if the temperature is sufficiently high causing the liquid–liquid phase separation. Moreover, like a concentrated polymer solution coexists in equilibrium with essentially pure water almost devoid of polymer molecules at temperatures sufficiently high, so does a concentrated salt solution coexist with essentially pure water, implying that the polymers in water solutions are charged, i.e., comprised of polymerised cations or anions. Further insights into the nature of polymers in aqueous electrolyte solutions with LCST are afforded by

correlating the corresponding ions with Hofmeister series.

Correlation of liquid immiscibility patterns with Hofmeister series. Franz Hofmeister observed at the end of the XIX century that various electrolytes had different effects on the stability of certain aqueous protein solutions. Some electrolytes would destabilize the solution inducing precipitation of the protein whereas others would enhance the solution stability. The ordering of ions according to their ability to destabilize/stabilise the protein solution has become known as Hofmeister series. Over the next hundred years Hofmeister series has been found to characterize the ions' ability (in decreasing or increasing order) to modify a plethora of phenomena, such as surface tension, zeta potential, pH in buffers, enzyme activity, bubble stability, among many others (Gregory et al., 2022).

Most authors order the ions in Hofmeister series as follows (stipulating the possibility of reversals for some ions, due to the counterion, pH, and the phenomenon under consideration),

anions: $CO_3^{2-} \approx H_2PO_4^{+} > SO_4^{2-} \approx HPO_4^{2-} > PO_4^{3-} > CH_3COO^{-} > F^{-} > Cl^{-} > Br^{-} > NO_3^{+} > I^{-} > ClO_4^{-} > CNS^{-}$

cations: $Bu_4N^{+} > Ca^{2+} > Mg^{2+} > Li^{+} > Na^{+} > K^{+} > NH_4^{+} > Me_4N^{+}$.

The exact mechanisms with which various ions influence in parallel so many different phenomena remain a mystery (Gregory et al., 2022). The ion's position in the series does not seem to correlate with any of its simple physical characteristics, such as charge, size, hydrophobicity etc., (Gregory et al., 2022). However, there is a thermodynamic quantity, the so-called water-structural entropy of ionic hydration, ΔS_{struct}, for which such a correlation is obvious. (Marcus, 2009) has shown that ions at the beginning of the Hofmeister series are characterized with large negative ΔS_{struct}, whereas ΔS_{struct} is positive for the ions from middle onwards. The quantity ΔS_{struct} is derived from the standard molar entropy of ion hydration by deduction of the entropic effect of a creation of a cavity in the water to accommodate the ion as well as the entropy of compression from the gaseous to the solution standard states and the contributions from the electrostatic effects. In essence, a negative value of ΔS_{struct} implies that dissolution of the ion diminishes the entropy of water.

Binary and triple water – salt systems with LCST are related to Hofmeister series, as follows: (1) liquid –liquid phase separation takes place solely with salts whose anions are at the beginning of Hofmeister series for anions (WO_4^{2-}, CO_3^{2-}, SO_4^{2-}, $H_2PO_4^{1-}$, HPO_4^{2-}, PO_4^{3-}); (2) for a fixed anion (sulfate) the value of T_{LCST} in the system decreases according to the position of the corresponding cation in Hofmeister series for cations ($Mg^{2+} < (UO_2)^{2-} < Li^{+} < Na^{+} < K^{+}$); (3) addition of a salt whose anion is located in the middle of Hofmeister series or closer to the end (Cl^{-} or ClO_4^{-}) to a water–salt system with LCST increases the liquid–liquid separation temperature, and the phase separation is suppressed completely at higher concentrations of these ions.

The nature of polymers responsible for phase separation. The aforementioned correlations imply that polymerization causing the liquid – liquid phase separation in aqueous electrolyte solutions is promoted by ions located in the beginning of Hofmeister series. At the same time these are the ions whose dissolution diminishes the entropy of water, as concluded by (Marcus, 2009). The large negative values of ΔS_{struct} obtained by (Marcus, 2009) are indicative of association (the entropy is reduced because aggregation of molecules reduces the number of translational, rotational and vibrational degrees of freedom). We see that ions from the beginning of Hofmeister series are precisely the ions promoting polymerization in the aqueous solution, and at the same as these are the ions causing water molecules to assemble into associates. This implies that the polymers and the associates are one and the same object, i.e., the polymers whose formation is promoted by ions from the beginning of Hofmeister series contain water molecules. These polymers, however, are not made up solely by water molecules because, as was pointed out above, ions also partake in polymerization. Therefore, charged heteropolymers comprised of ions and water molecules are to be present in aqueous solution experiencing liquid – liquid phase separation with LCST.

Fragments of a polyanionic chain in the crystal structure of $Na_2HPO_4 \cdot 12H_2O$. As is well-known, salt crystals grown from aqueous solutions often incorporate water molecules into their crystalline frameworks. If the polymers comprised of water molecules and ions responsible for liquid – liquid phase separation are present in the solution, these molecules or their fragments might be captured by a growing crystal and incorporated into the crystal framework. If such an incorporation does take place, finding an example of it in a deciphered crystal structure of a salt hydrate would prove indubitably the polymers' existence. To this end, an extensive search was made through the published crystal structures of hydrated salts comprised of cations and anions located at different sides of Hofmeister series. The search so far has been marked by a single successful find, remarkably, in a hydrated salt from a system Na_2HPO_4–H_2O in which a liquid – liquid

phase separation with LCST does take place.s

There are two polymorphs known for disodium hydrogenphosphate dodecahydrate. The structure of one of these, β-$Na_2HPO_4 \cdot 12H_2O$, which crystallises from water solutions below 30 ^{0}C, has been determined in (Templeton et al., 1990) and (Catti et al., 1978). Present in the structure are clusters of 12 water molecules and 8 HPO_4^{2-} groups tied together with hydrogen bonds, each cluster comprising a polyanion $[(HPO_4)_8(H_2O)_{12}]^{16-}$, Fig 5. The cluster is organized like a chain of 12 water molecules decorated with HPO_4^{2-} groups. Each water molecule partakes in three hydrogen bonds. Each H_2O molecule at the end of the chain is connected to one H_2O molecule (next to it in the chain) and two HPO_4^{2-} groups; each of the H_2O molecule inner to the chain is connected by hydrogen bonds to two molecules (adjacent to it in the chain) and to one HPO_4^{2-} group. The chain of water molecules in the cluster is not stretched but rather shaped as a compact globule.

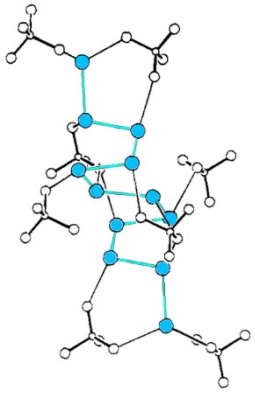

Fig. 5. The cluster comprising a chain of 12 water molecules surrounded by eight HPO_4^{2-} ions in the crystal structure of β-$Na_2HPO_4 \cdot 12H_2O$. Hydrogen bonds between water molecules are indicated by blue lines to emphasize the chain. Thin black lines indicate hydrogen bonds to phosphate groups. *Modified from* (Templeton et al., 1990).

The presence of the cluster $[(HPO_4)_8(H_2O)_{12}]^{16-}$ in the structure of β-$Na_2HPO_4 \cdot 12H_2O$ confirms the hypothesis proposed above ascribing liquid – liquid immiscibility phenomenon to formation of linear polymerss in aqueous solutions. The cluster is a fragment of a linear polymer (an oligomer) made up of water molecules and anions from the beginning of Hofmeister series. Obviously, it matches the description of polymers present in solutions deduced above. The oligomers could have been severed from larger polyanionic molecules present in the solution. The observed globular configuration of the $[(HPO_4)_8(H_2O)_{12}]^{16-}$ clusters suggests a plausible explanation of their extremely rare occurrence in the hydrated salt crystals. When the long polymer chains made up of water molecules and ions interact with the surface of a growing crystal, they most probably tend to break into oligomers and fold into compact globules. Integrating such globular ions into a crystal structure is energetically challenging.

Conclusions. Apparent similarities between liquid – liquid immiscibility phenomena in water – salt systems with LCST and liquid – liquid immiscibility in polymer solutions signify the presence of linear polymers in aqueous electrolyte solutions. Just like in polymer solutions, phase separation occurs in aqueous electrolyte solutions when these polymers experience a coil-to-globule transition. These polymers are charged molecular chains comprised of water molecules and the ions located at the beginning of Hofmeister series. Though marked with impressive thermodynamic stability, implied by their presence in liquid and subcritical fluid solutions at temperatures ranging from 30 to 800 ^{0}C, it is only in rare instances that these polymers are incorporated into crystal structures of salt hydrates, presumably because once in contact with the surface of a crystal they assume a globule conformation.

Acknowledgements. *I am grateful to Prof. E.G. Osadchii's whose unflagging attention and interest stimulated the appearance of the present publication. I also thank Prof. A. F. Redkin for providing data on liquid–liquid equilibrium in the system NaF–H_2O.*

References

Aladko L., Dyadin Yu. (1994) Clathrate Formation and Retrograde Miscibility of Liquids in the Bu_4NF–NH_4F–H_2O System. Mendeleev Communications. 4. 67-68.

Catti M., Ferraris G. Ivaldi G. Disorder of HPO_4^{2-} and of hydrogen bonds in the structure of β-$Na_2HPO_4.12H_2O$. *Acta Cryst.* (1978). B34, 369-373

Crespy D., Rossi R.M. Temperature-responsive polymers with LCST in the physiological range and their applications in textiles. Polym. Int., 56 (2007), pp. 1461-1468

Cui et al., 2021. Melt–Fluid and Fluid–Fluid Immiscibility in a Na_2SO4–SiO_2–H_2O System and Implications for the Formation of Rare-Earth Deposits. Acta Geologica Sinica (English Edition), 95(5): 1604–1610.

Diab C., Akiyama Y., Kataoka K., Winnik F.M. Microcalorimetric study of the temperature-induced phase separation in aqueous solutions of poly(2-isopropyl-2-oxzolines). *Macromolecules* 2004, 2556–2562.

Gregory K P, Elliott G R, Robertson H, Kumar A, Wanless E J, Webber G B, Craig V S J, Andersson G G and Page A J 2022 Understanding specific ion effects and the Hofmeister series Phys. Chem. Chem. Phys. 24 12682–718

Heskins M., Guillet J. E. Solution Properties of Poly(N-isopropylacrylamide). *J. Macromol. Sci.-Chem.*, A2, 1441 (1968).

Kotel'nikova Z.A., Kotel'nikov A.R. Immiscibility in sulfate-bearing fluid systems at high temperatures and pressures. *Geochem. Int.* 48, 381–389 (2010).

Kujawa P., Winnik F.M.Volumetric studies of aqueous polymer solutions using pressure perturbation calorimetry: A new look at the temperature-induced phase transition of poly(N-isopropylacrylamide) in water and D_2O. Macromolecules 34 (2001) 4130.
Marcus Y. Effects of ions on the structure of water: structure making and breaking. *Chem. Rev.* 2009, 109, 3, 1346–1370
Marshall W.L. Two-liquid-phase boundaries and critical phenomena at 275–400 °C for high-temperature aqueous potassium phosphate and sodium phosphate solutions. Potential applications for steam generators, J. Chemical and Engineering Data 27 (1982) 175–180.
Marshall W. L. Aqueous inorganic phase equilibria at high temperatures: some experimental, theoretical, and applied aspects. *Pure & Appl. Chem.,* Vol. 57, No. 2, pp. 283—301, 1985.
Marshall W.L., Gill J.S. Effects of pressure on liquid-liquid immiscibility of high temperature aqueous solution mixtures of uranyl sulfate and sulfuric acid, 280–450ºC, 75–1800 bars, J. Inorg. Nucl. Chem. 36 (1974) 2303–2312.
Marshall W.L., Hall C.Y., Mesmer R.E.. The system dipotassium hydrogen phosphate – water at high temperatures (100-400°)); liquid – liquid immiscibility and concentrated solutions. J. inorg. Nucl. Chem. Vol. 43, pp. 449-455 (1981)
D. Patterson, G. Delmas, T. Somcynsky. A comparison of lower critical solution temperatures of some polymer solutions. Polymer, Volume 8, Pages 503-516. (1967)
Ravich M.I. and Borovaya F.E. Zh. Neorg. Chim., 9, 952-974 (1964).
Redkin A.F., Kotova N.P. Shapovalov Y.B. Liquid immiscibility in the system NaF–H_2O and microlite solubility at 800°C. *Dokl. Earth Sc.* 469, 722–727 (2016).
Reimer J., Vogel F. High pressure differential scanning calorimetry of the hydrothermal salt solutions K_2SO_4–Na_2SO_4–H_2O and K_2HPO_4–H_2O. *RSC Adv*. 3 (2013) 24503–24508.
Reimer J., Vogel F. Influence of anions and cations on the phase behavior of ternary salt solutions studied by high pressure differential calorimetry. The Journal of Supercritical Fluids 109 (2016) 141-147.
Saeki, S.; Kuwahara, N.; Konno, S.; Kaneko, M. Pressure dependence of upper and lower critical solution temperatures in polystyrene solutions. Macromolecules 1973, 6 (2), 246−250.
Templeton D.H., Ruben H., Zalkin A. (1990). Entropy and crystal structure of hydrates of disodium hydrogen phosphate. *The Journal of Physical Chemistry, 94*, 7830-7834.
Urusova M.A., Valyashko V.M. Solubility of NaF and Li_2CO_3 salts of the 2nd type in supercritical water and solutions of aqueous electrolytes (NaCl, Na_2WO_4, and Li_2SO_4). *Russ. J. Phys. Chem. B* 8, 919–923 (2014).
Urusova M., Valyashko V. (2019) Phase Equilibria in the $ZnSO_4$–H_2O System at Temperatures to 444°C and Pressures to 34 MPa. Russian Journal of Inorganic Chemistry. 64. 401-406.
Urusova M.A., Valyashko V.M., Grigor'ev I.M. K_2SO_4–KCl–H_2O phase diagram in the area of heterogenization of homogeneous supercritical fluids. Russian Journal of Inorganic Chemistry (2007) 52(3):405-418.
Wang X., Chou I-Ming, Hu W., Burrus R.C. (2013) In situ observations of liquid–liquid phase separation in aqueous $MgSO_4$ solutions; Geological and geochemical implications. *Geochimica et Cosmochimica Acta 103 1 – 10*.
Wan Y., Wang X., Hu W., Chou I-M., Wang X., Chen Y., Xu Z. (2017) In situ optical and Raman spectroscopic observations of the effects of pressure and fluid composition on liquid–liquid phase separation in aqueous cadmium sulfate solutions (400°C, 50 MPa) with geological and geochemical implications. Geochimica et Cosmochimica Acta 211 (2017) 133–152.
Wolf B.A. Improvement of polymer solubility: Influence of shear and of pressure. Pure & Appl. Chem., Vol. 69, No. 5, pp. 929-933, 1997.
Zhang Q, Weber C, Schubert US, Hoogenboom R. Thermoresponsive polymers with lower critical solution temperature: from fundamental aspects and measuring techniques to recommended turbidimetry conditions Materials Horizons. 4: 109-116 (2017).

Bublikova T.M., Setkova T.V., Balitsky V.S. Stability conditions and solubility of solid phases in the CuO – CO_2 – H_2O system at temperatures up to 100 °C *UDC 553.4:549.01:549.743*

D.S. Korzhinskii Institute of Experimental Mineralogy RAS, Chernogolovka e-mail: tmb@iem.ac.ru

Abstract. In the CuO–CO_2–H_2O system, phase equilibria were calculated and solubility diagrams of compounds were plotted at temperatures of 25–100 °C using the geochemical modeling method. The stability conditions for tenorite, malachite, azurite and the compositions of solutions in equilibrium with them under the conditions of the oxidation zone of sulfide copper and polymetallic deposits were determined. The role and quantitative contribution of species of an aqueous solution to the formation of solid phases of the system depending on the temperature and partial pressure of carbon dioxide were established. The results of the calculations showed that at the deeper horizons of the oxidation zone, the deposition of malachite and azurite is accursed from solutions richer in copper.

Keywords: thermodynamic modeling, copper, tenorite, malachite, azurite, phase formation, oxidation zone, solubility diagrams

Among more than two hundred copper minerals known in nature, only about forty are of industrial importance. The copper minerals tenorite, malachite and azurite, widely distributed in the zone of oxidation of copper sulfide and polymetallic deposits, are among the 15 most important for industry. Factors such as: the chemical situation and environmental risks in the areas of mining and processing plants, copper contamination of surface

watercourses, copper corrosion processes are closely related to determining the conditions for the formation and stability of these minerals. The use of the thermodynamic modeling method makes it possible to obtain information about the conditions for the formation of copper minerals, the composition of the solution, and chemical processes occurring during the interaction of solid and liquid phases with a change in thermobaric parameters.

The phase formation of copper oxide and carbonates in the Cu^{2+}– CO_2 – H_2O system at atmospheric pressure and low temperatures (T = 280–350 K) was most fully considered by W. Preis and H. Gamsjager (Preis and Gamsjager, 2002). The presented three-dimensional stability diagram for compounds of the Cu^{2+}–CO_2–H_2O system was calculated using new thermodynamic data obtained by the authors. The reliability of the obtained thermodynamic characteristics is confirmed by the results of experiments on the transformation of tenorite into malachite and the synthesis of azurite. The set of thermodynamic values calculated on the basis of experimental data is in good agreement with the previously obtained data on the solubility of malachite and azurite (Silman, 1958; Schindler et al., 1968; Symes, Kester, 1984). The results of a theoretical study of phase formation in the Cu–H_2O– system with the participation of a number of species of an aqueous solution (including the CO_3^{2-} -ion) (Puigdomenech I., Taxén C., 2000) have great practical importance. The work was carried out by the authors in connection with the study of the corrosion processes of copper containers in the planned storage facilities for spent nuclear fuel. The chemical composition of the model solution corresponded to the composition of groundwater in Swedish granites at a depth of about 500 meters. The authors showed the possibility of formation of tenorite and malachite under conditions similar to those existing in the places of burial of spent nuclear waste in granites of Sweden and their role in corrosion processes on the outer surface of copper containers. at temperatures of 25, 100 °C.

The presented diagrams of the stability of compounds in aqueous copper-carbonate systems make it possible to judge the stability of tenorite and malachite at temperatures of 280–373.15 K, azurite at 293.15–323.15 K, in a wide range of solution pH. Similar conditions are observed in the surface part of the oxidation zone. However, the cited papers present state diagrams calculated at a constant molar fraction of copper: 10^{-4} mol/l (Preis, Gamsjager, 2002) and 10^{-6} mol/kg (Puigdomenech, Taxén, 2000). There are very few data in the literature that could quantitatively characterize the processes of copper oxide and carbonate deposition in the oxidation zone. The analyzes given in the articles for the content of copper in mine waters differ by an order of magnitude or more. Thus, the waters of the polymetallic deposits of Central Kazakhstan contain 2.10^{-4} g/l of copper (Smirnov, 1955); the concentration of copper in the mine waters of the South Urals deposits ranges from 46.1 at the Uzelga deposit to 1920 mg/dm^3 at the Gaiskoye deposit. At the Uzelga deposit, in the area of direct mining in mine workings, the copper content in water reaches 175 mg/dm^3 (Orekhova, 2015).

The objectives of this study were included: determination of the conditions for phase formation and interaction of solid phases with the solution, assessment of its composition and forms of copper transfer under conditions typical for the oxidation zone of copper sulfide deposits. The CuO–CO_2–H_2O system was chosen as the model system.

Thermodynamic calculations of mineral equilibria were carried out using the HCh geochemical modeling program (Shvarov and Bastrakov, 1999). When compiling the database, special attention was paid to the harmonization of thermodynamic quantities. To calculate the Gibbs free energy of species of an aqueous solution at elevated temperatures, we used the equations of B.N. Ryzhenko (Ryzhenko, 1981) and Helgeson-Kirkham-Flowers (Helgeson, Kirkham, Flowers, 1981). The thermodynamic functions of malachite and azurite were calculated using the heat capacity equations obtained by us earlier (Bublikova et al., 2000).

The phase diagrams of the solubility of copper compounds are calculated for temperatures of 25–100 °C and a pressure of 0.1 MPa. The total amount of water in the solution is constant and equal to 1 kg. Isothermal diagrams of the solubility of the CuO–CO_2–H_2O system for temperatures of 25, 50, 75, 100 °C are shown in fig. 1; the concentration of aqueous copper species in solutions in equilibrium with solid phases at temperatures of 25 and 100 °C is shown in fig. 2. As can be seen from fig. 1, under atmospheric conditions (T=25 °C, p_{CO2} $\approx 10^{-3.45}$ atm), the formation of tenorite is most likely; tenorite and malachite are resistant to azurite. For the formation of copper carbonates, additional introduction of carbon dioxide into the solution is necessary. Its source under natural conditions is groundwater, atmospheric CO_2 and bicarbonate solutions. The species of the solution $CuOH^+$, Cu^{2+} dominate the regions of almost pure water (log $p_{CO2} \approx 7$). The total concentration of copper increases with an increase in the partial pressure of CO_2. Its content in a solution in equilibrium with malachite ranges from $2.7 \cdot 10^{-5}$ to $4.4 \cdot 10^{-4}$ mol/kg, with azurite - from $4.4 \cdot 10^{-4}$ to $2.2 \cdot 10^{-3}$ mol/kg. Forms of copper transfer: Cu^{2+}, $CuOH^+$, $CuHCO_3^+$, $CuCO_3^0$ (Fig. 2). The content of carbonate-bicarbonate species $CuHCO_3^+$, $CuCO_3^0$ increases with the increase of CO_2 concentration in

the solution, while the content of aqueous species $CuOH^+$, $Cu(OH)_2^0$ decreases. The total concentration of species of the $Cu(OH)_2^0$, CuO_2^{2-}, $Cu(OH)_3^-$, $Cu_2(OH)_2^{2+}$, $Cu_3(OH)_4^{2+}$, $Cu(CO_3)_2^{2-}$, $Cu(OH)_4^{2-}$ solution is less than 0.1 % and does not make a significant contribution to the total amount of dissolved copper.

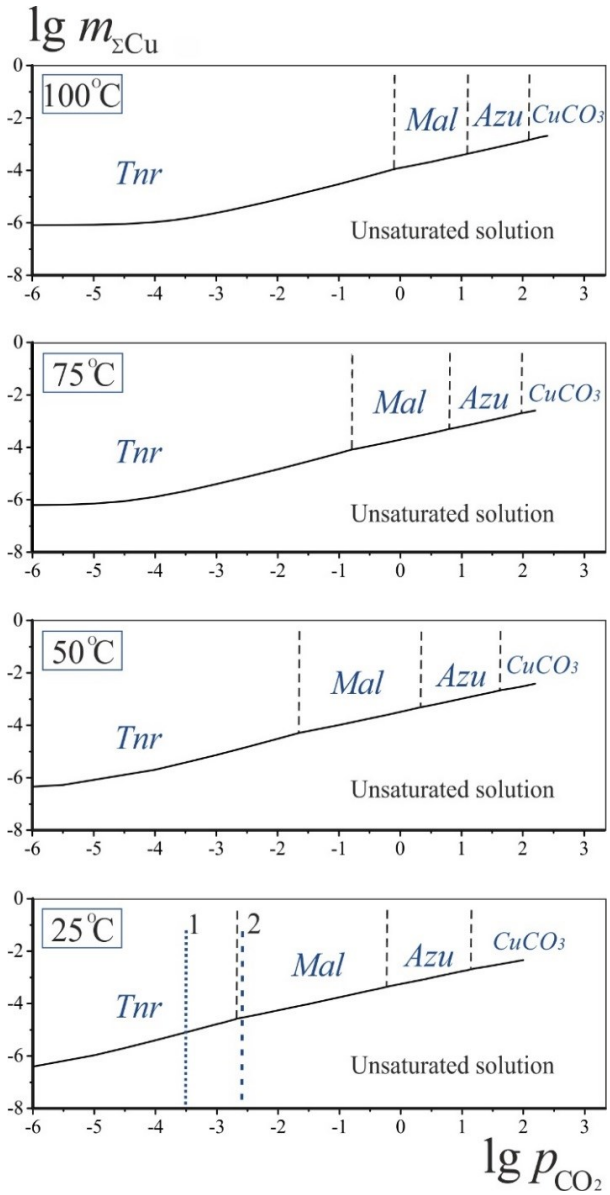

Fig.1. Isothermal diagrams of the solubility of copper compounds in the $CuO–CO_2–H_2O$ system. T=25, 50, 75, 100 °C; P=0.1 MPa. ***Tnr*** - tenorite; ***Mal*** - malachite; ***Azu*** - azurite. 1 – partial pressure of CO_2 under atmospheric conditions; 2 - CO_2 content in rainwater.

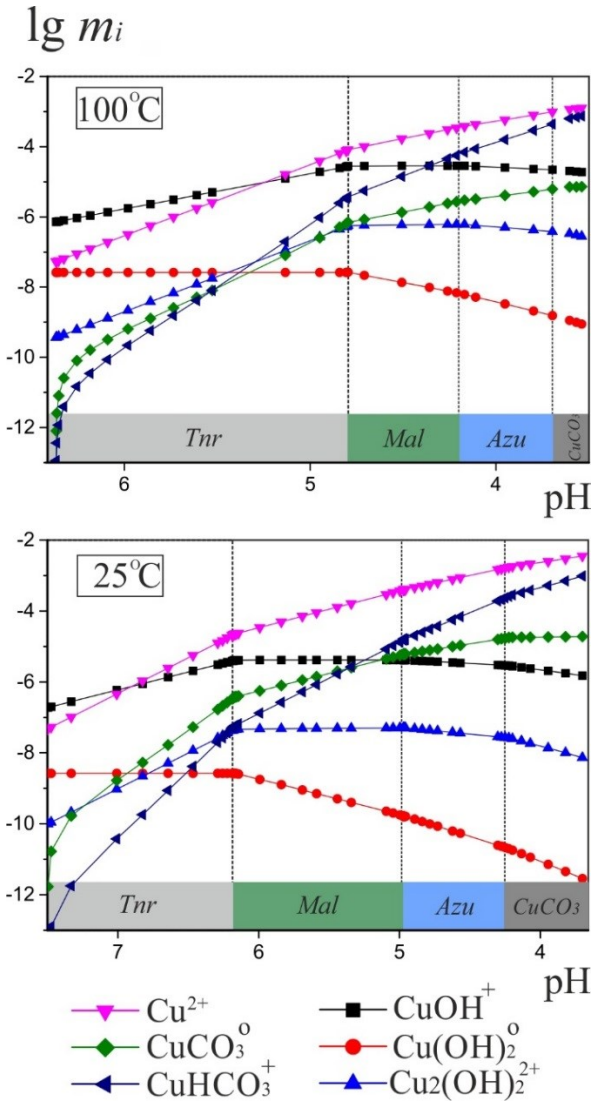

Fig. 2. The concentration of copper species in a solution in equilibrium with solid phases (mol/kg) depending on pH at temperatures of 25 and 100 °C; P=0.1 MPa.

The results obtained allow us to explain the process of formation of the so-called "copper greenery" on the surface of copper roofs of buildings and archaeological objects made of bronze under atmospheric conditions (Nienhuis et al., 2016). According to Reichardt, atmospheric precipitation is highly enriched in carbon dioxide (Smirnov, 1955), since the air dissolved in rainwater contains 10 vol. % carbon dioxide, in contrast to atmospheric (0.03 - 0.045 vol.%). On figure 1 (see Fig. 1, T=25 °C), the dashed line indicates the partial pressure of carbon dioxide, corresponding to its concentration in rainwater, equal to 1.34×10^{-4} mol/l. It follows from the analysis of the diagram that, under conditions of a sufficient amount of copper, upon its contact with rainwater, the formation of a malachite phase is likely and regular.

As the temperature rises to 100 °C, the shape of the isotherm does not change significantly (Fig. 1, T=50, 75, 100°C). The absolute values of the equilibrium concentration of copper in solution at a constant CO_2 pressure decrease in the temperature

range of 25–100 °C. The general character of the change in the concentration of copper species practically does not change. The concentration of copper in a solution in equilibrium with malachite is higher: $1.15 \cdot 10^{-4}$ – $4.88 \cdot 10^{-4}$, with azurite - from $4.84 \cdot 10^{-4}$ to $1.90 \cdot 10^{-3}$ mol/kg towards the boundary of equilibrium with copper carbonate. Thus, the calculated data show that at the deeper horizons of the oxidation zone, the deposition of malachite and azurite occurs from the solutions most saturated with copper. The calculated data obtained are in good agreement with the results of a study of the mineralization of mine waters of the Levikhinsky copper pyrite deposit (Middle Urals). Depending on the lowering of the horizon from 85 to 205 m, the copper content in water increases from 125 to 2548 mg/l (Rybnikova et al., 2014).

The stability fields of malachite and azurite shift to higher values of partial pressure of CO_2 and lower values of solution pH with increasing temperature. Thus, the effect of temperature on the stability of the phases in the system under consideration is to increase the stability of tenorite due to malachite and malachite due to azurite.

This study is fulfilled under Research program № FMUF-2022-0002 of the Korzhinskii Institute of Experimental Mineralogy

References

Bublikova T.M., Balitsky V.S., Timokhina I.V. Synthesis and main properties of jewelry and ornamental malachite. Synthesis of minerals. V. 1. Alexandrov, VNIISIMS. 2000. 662 p. (In Russian).

Helgeson H. C., Kirkham D. H., and Flowers G. C. Theoretical prediction of the thermodynamic behavior of aqueous electrolytes at high pressures and temperatures: IV. Calculation of activity coefficients, osmotic coefficients, and apparent molal and standard and relative partial molal properties to 600 °C and 5 kb. Am. J. Sci. 1981. 281. 1249–1516.

Nienhuis J., Robbiola L., Giuliani R., Joosten I., Huisman H., Bertil van Os, Sietsma J. Curly malachite on archaeological bronze. e-PS. 2016. 13. 23–32.

Orekhova N.N., Shadrunova I.V. Formation and complex processing of natural and technogenic waters during the exploitation of copper-zinc pyrite deposits. Magnitogorsk: Magnitogorsk Publishing House. State tech. un-ta im. G.I. Nosov. 2015. 185 p.

Preis W., Gamsjager H. Solid-solute phase equilibria in aqueous solution. XVI. Thermodynamic properties of malachite and azurite. Predominance diagrams for the system Cu – H_2O – CO_2. J. Chem. Thermodynamics. 2002. 34. 631–650.

Puigdomenech I., Taxén C. Thermodynamic data for copper. Implications for the corrosion of copper under repository conditions. Technical Report TR-00-13. 2000.

Rybnikova L.S., Rybnikov P.A., Tyutkov O.V. Assessment of the impact of flooded copper pyrite mines on water bodies in the Middle Ural. Water management of Russia. 2014. 6. 77–91.

Ryzhenko B.N. Thermodynamics of equilibrium in hydrothermal solutions. M.: Science. 1981. 191 p.

Schindler P., Reinert M., Gamsjager H. Helv. Chim. Acta. 1968. 51. 1845–1856.

Shvarov Yu.V., Bastrakov E. HCh: a Software Package for Geochemical Equilibrium Modeling: User's Guide (AGSO RECORD 1999/y). Canberra: Austr. Geol. Surv. Organisation; Dept. Industry, Science and Resources. 1999. 57 p.

Smirnov S.S. Zone of oxidation of sulfide deposits. L: Ed. Academy of Sciences of the USSR. 1955. 231 p.

Symes, J. L., Kester D. R. Geochim. Cosmochim. Acta. 1984. 48. 2219–2229

Kovalev V.N.[1], Thomas V.G.[2], Setkova T.V.[3], Zubkova N.V.[1], Spivak A.V.[3], Fursenko D.A.[2] Crystal growth of phenakite-like solid solution and structural spectroscopic study

UDC 548.55, 548.545, 549.057, 549.621.21

[1] The Faculty of Geology, Lomonosov Moscow State University; [2] Sobolev Institute of Geology and Mineralogy SB RAS, [3] Korzhinski Institute of Experimental Mineralogy RAS (IEM RAS), kovvn99.msu16@gmail.com;

Abstract. Single crystals of $Be_2(Si_{1-x}Ge_x)O_4$ with phenakite structure (x = 0-0.25 and 0.80, 1) have been synthesized by hydrothermal method (T_1/T_2 = 580/660°C, P = 150 MPa) for the first time. It was shown that the use of LiF-containing solutions promotes the formation of single crystals, while the use of solutions NaF-containing solutions leads to the passivation of germanium with the formation of insoluble germanates. Results of X-ray diffraction analysis of $Be_2(Si_{1-x}Ge_x)O_4$ representatives with x = 0, 0.80 and 1 illustrated linear changes in unit cell parameters and Si(Ge)-O bond lengths with increasing germanium content in the crystal. The use of temperature-induced zoning technique resulted in the formation of zoned single crystals with a germanium content range of $0.04 < x < 0.25$. Raman spectroscopy in that range of germanium content showed a linear shift of band positions to lower frequencies with increasing germanium content.

Keywords: phenakite, germanium, hydrothermal synthesis, Raman spectroscopy, X-Ray structural analysis

The interest to investigation of germanium-rich analogues of the mineral such as phenakite (natural beryllium orthosilicate Be_2SiO_4) is explained by the several reasons. First, this mineral is an industrially significant beryllium source in fluorite-phenakite deposits (Kostov, 1971). Secondly, the specific features of polyhedron interconnection and electron density distribution in the phenakite crystal structure contribute to the appearance of the properties of a promising optical material (Kaminskii et al., 2014).

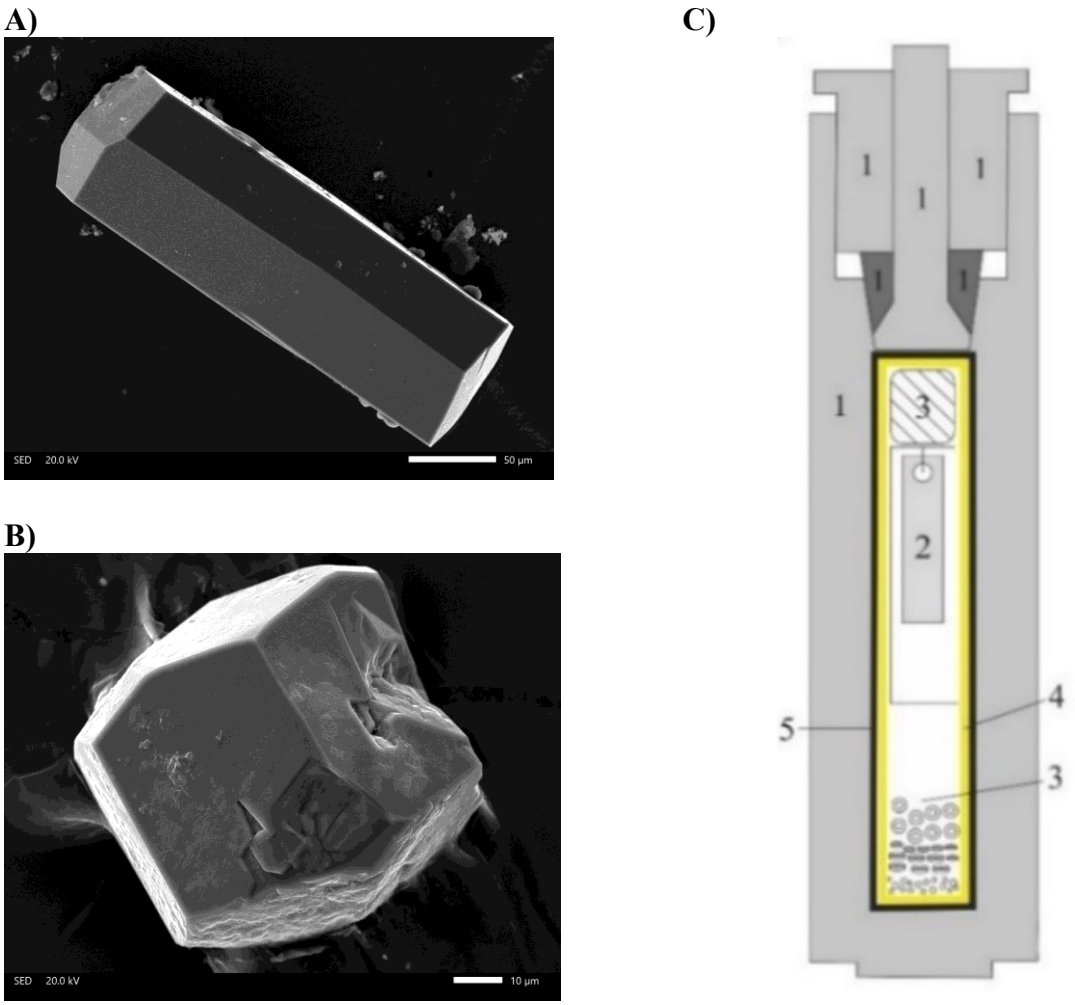

Figure 1. A) Phenakite single crystal Be_2SiO_4; B) Single crystal of $Be_2(Si_{1-x}Ge_x)O_4$ with x = 0.80; C) the loading scheme of the autoclave used for synthesis of single crystalline solid solution $Be_2(Si_{1-x}Ge_x)O_4$. Notations: 1 - body and parts of the autoclave, 2 - seed, 3 - charge, 4 - gold liner, 5 - supporting fitting.

It is well known that the properties of silicates can be modified by the incorporation of germanium impurities. Such isomorphism leads to formation of solid solutions - compounds of mixed composition possessing superior (in comparison with pure silicates) physical properties. Similar phenomena were observed for synthetic analogues of quartz, tourmaline and topaz (Balitsky et al., 2004; Spivak et al., 2021; Borovikova et al., 2023). In this regard, it is interesting to obtain and study germanium-rich analogues of phenakite of $Be_2(Si_{1-x}Ge_x)O_4$ and their complex physical chemical investigations.

The currently published investigations were mostly focused on the polycrystalline samples (powders) of solid solution with phenakite crystal structure, and the authors obtained both extreme members, as well as compounds of intermediate composition (Kortov et al., 1985). In the present study, single crystals of solid solution with the phenakite crystal structure $Be2(Si_{1-x}Ge_x)O_4$ were obtained for the first time (Figure1A,B). Synthesis of these single crystals was carried out in autoclaves (Figure 1C) by hydrothermal method with direct temperature difference. The experiments were carried out at T_1/T_2 = 580/660°C and P = 150 MPa. Two types of complex solutions were used: sodium fluoride-based NaF and LiF-based. Both types of solutions have been used before and are currently used for the synthesis of another important beryllium silicate, beryl (Thomas, Lebedev, 1982).

The selection of the composition of hydrothermal solution fundamentally affected the results of the experiments. In experiments with NaF-containing solutions only Be_2SiO_4 phenakite single crystals were obtained (Figure 1A), whereas experiments with LiF-containing solutions yielded solid solution single crystals with x = 0, 0.80 and 1 (Figure 1B). Similar results were noted earlier, for example, in work (Balitsky et al., 2004) where use of Na-containing mineralizers led to passivation of dissolved germanium by formation of poorly soluble sodium germanates. Change of hydrothermal solution

components also affected the morphology of obtained crystals. In experiments using LiF-containing solutions the crystals are characterized by less elongation with the same crystal habit. In experiments using LiF-containing solutions the crystals are characterized by less elongation with the same crystal habit.

Obviously, the change of morphology of the obtained crystals is caused by the change of ratios of growth rates of habitus faces, in our case by the increase of face growth rate of hexagonal prism m {10-10}.

Since no structural data were available for the solid solution $Be_2(Si_{1-x}Ge_x)O_4$, the structural analysis of the solid solution members with x = 0.80 and 1 was carried out; for reliability of the subsequent statistical processing the structural analysis was also carried out for the member with x = 0 (pure phenakite). The structural analysis was carried out within the *R*-3 space group, which is typical for minerals of the phenakite group. As a result of the analysis we obtained the following patterns (Figure 2, Figure 3 A, B).

The compounds with phenakite structure T'2T''O4 are framework heterosilicates T'[T''O4] (T' - position of divalent element, T'' - position of quadrivalent element; in our case T' = Be, T'' = Si, Ge). As the fraction of germanium in the T'' position increases, the bond length T''-O in the tetrahedron $T''O_4$ increases. This dependence is linear. Consequently, the parameters a(=b) and c (Figure 3A) and the unit cell volume V (Figure 3B) increase linearly with increasing interatomic distance.

The hydrothermal experiments were also carried out using the technique of induced temperature zoning, previously widely used to study flux (Damen and Robertson, 1972) and hydrothermal (Thomas et al., 1999) systems. The same PT conditions of experiments mentioned earlier were used in application of this technique. The essence of this technique is the regular short-term switching off the heater of the growth unit for a fixed time interval (30 minutes). As a result of this technique, we obtained zonal solid solution single crystals (Figure 4A). The zoning in the crystals is an alternation of narrow and wide bands, with the formation of narrow bands timed to coincide with heater shutdowns.

The contrast distribution of the germanium impurity over the slice surface of such a zonal crystal is of interest for spectroscopic and statistical analysis, which have not been carried out so far for the solid solution $Be_2(Si_{1-x}Ge_x)O_4$. Raman spectroscopy was used as the major method for the analysis.

Raman spectra from a zonal crystal sample (Figure 4B) were collected in each wide zone, the analysis points are shown in Figure 4A; the chemical compositions were also determined at these points to assess the peak position-composition correlation.

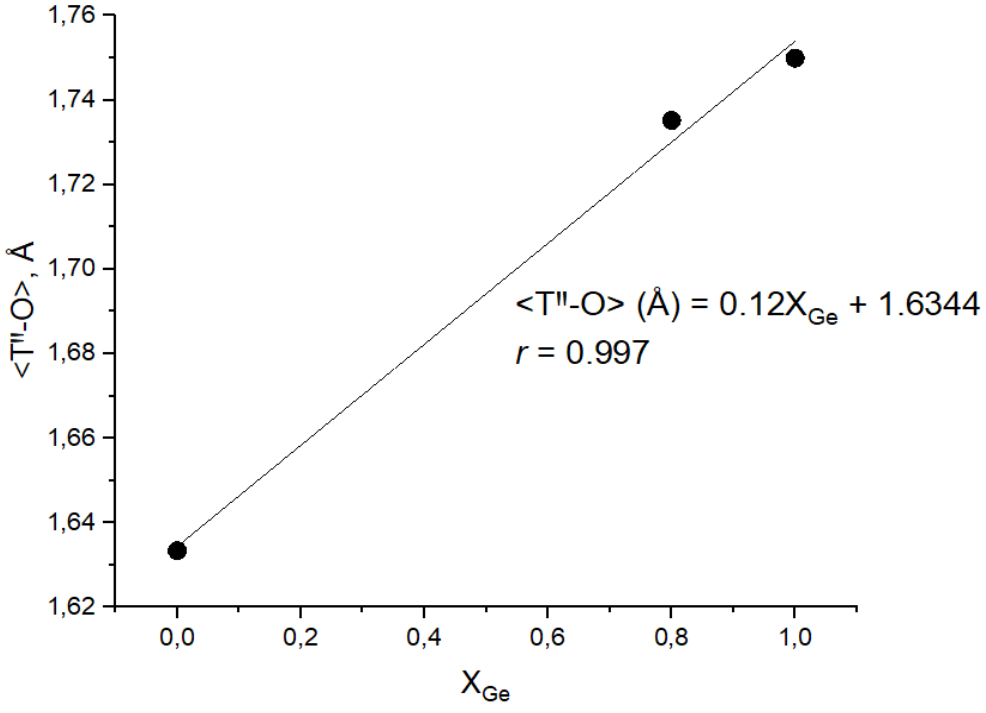

Figure 2. The change in bond length <T''-O> as a function of X_{Ge}.

A) **B)**

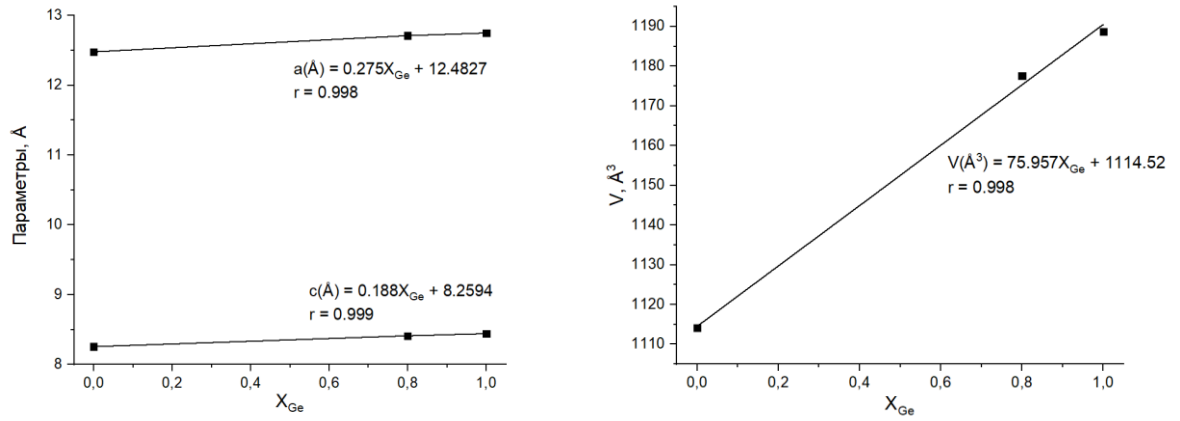

Figure 3. Changes in unit cell parameters a(=b), c (A) and V (B) as a function of X_{Ge}.

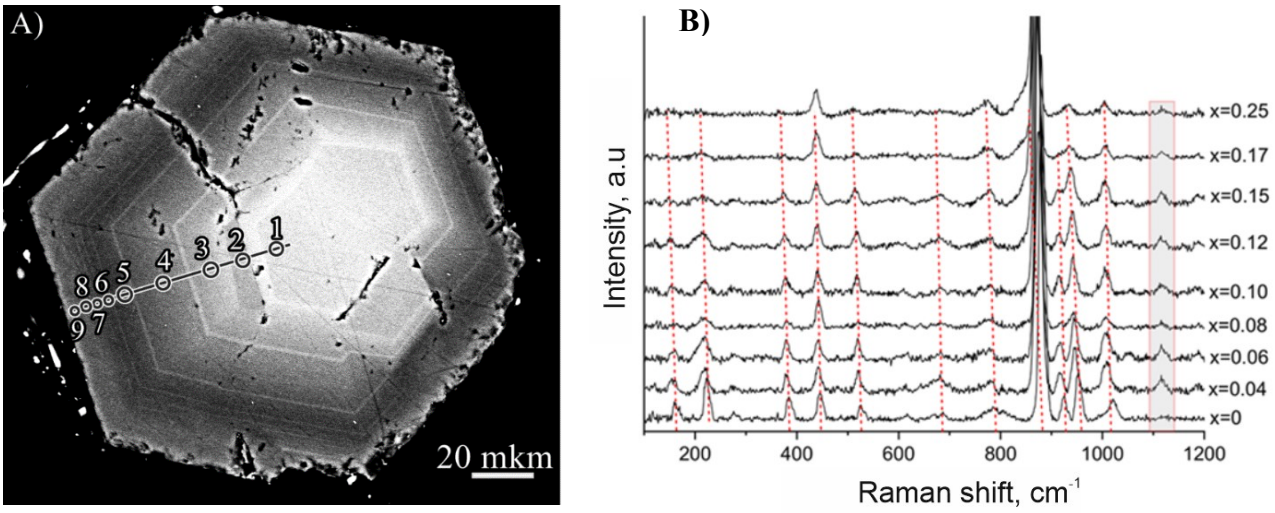

Figure 4. A) Zonal single crystal of $Be_2(Si_{1-x}Ge_x)O_4$ with contrasting distribution of germanium on the crystal surface (1 - x = 0.25, 9 - x = 0); B) Raman spectra of $Be_2(Si_{1-x}Ge_x)O_4$ as a function of X_{Ge}.

The bands shift to a lower frequencies as the germanium content increases. The trend lines of the shifts are straight lines. Thus, the dependence of the band shift in the Raman spectra of $Be_2(Si_{1-x}Ge_x)O_4$ is close to linear and can be described by the following equation: $\Omega = AX_{Ge} + B$. By the linear regression analysis, the coefficients A and B corresponding to each of the bands were determined and given in Table 1.

Ω_0, cm^{-1}	*Type*	*Intercept coefficient **B***		*Slope coefficient **A***	
		Value	*Confidence interval*	*Value*	*Confidence interval*
879	A_g	0.996	±0.001	-0.057	±0.009
787	A_g	0.995	±0.002	-0.084	±0.016
952	A_g	0.997	±0.001	-0.082	±0.008
1020	A_g	0.993	±0.002	-0.061	±0.017
161	E_g	0.999	±0.007	-0.467	±0.052
222	E_g	0.994	±0.004	-0.259	±0.030
384	E_g	0.999	±0.001	-0.171	±0.009
446	E_g	0.995	±0.002	-0.093	±0.013
523	E_g	0.996	±0.001	-0.113	±0.011
928	E_g	0.995	±0.002	-0.090	±0.026
687	E_g	0.997	±0.001	-0.071	±0.008

Each of the shift trend lines is described by correlation coefficient |R| > 0.8, indicating close to

linear pattern of the shift.

Hence, $Be_2(Si_{1-x}Ge_x)O_4$ crystals were first synthesized by hydrothermal method (T1/T2 = 580/660℃, P = 150 MPa) using LiF-containing solutions. X-ray diffraction study of solid solution representatives with x = 0, 0.80 and 1 revealed a linear increase in structural parameters with increasing germanium content. Raman spectroscopic analysis of zonal crystal with $0 < x < 0.25$ showed linear shift of bands to lower frequencies with increase of germanium content in crystal.

This study is fulfilled under Research program FMUF-2022-0002 of the Korzhinski Institute of Experimental Mineralogy.

The authors are grateful to V.O. Yapaskurt (MSU) and S.G. Simakin (YarGU) for analytical studies of the compositions of the grown crystals.

References

1. V. S. Balitsky, D. V. Balitsky, A. N. Nekrasov, L. V. Balitskaya, G. V. Bondarenko, and O. L. Samokhvalova. Growth, Structural–Morphological Features, and Some Properties of Quartz–Germanium Oxide Solid Solution Monocrystals with Quartz Structure // Doklady Earth Sciences. 2004. 396(1). 89–92.
2. Ivan Kostov. Mineralogy. – Oliver and Boyd, 1968, 587 p.
3. V.G. Thomas, A.S. Lebedev. Kinetics of hydrothermal crystallization of beryl from oxides. Fisiko-khimicheskiye issledovaniya mineraloobrazuyuschikh system. Inst Geologii i Geofiziki, 1982, pp. 98–104 (in Russian).
4. Borovikova E.Yu., Spivak A.V., Setkova T.V., Kvas P.S., Kuzmin A.V., Zakharchenko E.S., Balitsky V.S., Khasanov S.S., Lazarenko V.A., Dorovatovskii P.V., Korshunov D.M., Aksenov S.M. Synchrotron Single-Crystal XRD, IR-, Raman Spectroscopy and High Pressure Study of Synthetic Krieselite // Spectrochimica Acta - Part A: Molecular and Biomolecular Spectroscopy. 2023. 288(5). 122137.
5. Damen J.P., Robertson I.M. Induced Non-Periodic Growth Striations in Flux Grown Magnetic Oxide Single Crystals // Journal of Crystal Growth. 1972. 16(1). 50–53.
6. Kaminskii A.A., Lux O., Rhee H., Eichler H-J., Yoneda H., Shirakawa A., Becker P., Bonaty L. Beryllium Silicate, Be2SiO4 (phenakite) – a Novel Trigonal SRS-Active Crystal // Laser & Photonics Reviews. 2014. 8. 324–331.
7. Kortov, V.S., Zatsepin, A.F., Ushkova, V.I. Exoelectron Spectroscopy of Traps in Surface Layers of Phenakite and Quartz // Physics and Chemistry of Minerals. 1985. 12. 114–121.
8. Spivak A.V, Borovikova E.Y, Setkova T.V. Raman Spectroscopy and High Pressure Study of Synthetic Ga,Ge-Rich Tourmaline // Spectrochimica Acta A: Molecular and Biomolecular Spectroscopy. 2021. 248. 119171.
9. Thomas V.G., Demin S.P., Foursenko D.A., Bekker T.B. Pulsation Processes at Hydrothermal Crystal Growth (Beryl as Example) // Journal of Crystal Growth. 1999. 206. 203-214.

Rubtsova E.A.[1] , Akinfiev N.N.[1], Zotov A.V.[1], Tagirov B. R.[1] Experimental modeling of Pd transport by sulfide hydrothermal fluid *UDC 550.4.02*

[1] Institute of Geology of Ore Deposits, Petrography, Mineralogy and Geochemistry Russian Academy of Sciences (IGEM RAS) *rkata@mail.ru*

Abstract. The solubility of $PdS_{(cr)}$ (*vysotskite*) was measured in aqueous H_2S (0.1-2.0*m*, mol/kg H_2O) and H_2S + NaOH (0.02-0.4*m* H_2S + 0.05-0.4*m* NaOH) solutions at 4, 25, 75°C, 1 bar and at 450, 490°C, 1000 bar. The values of the Gibbs free energies of $Pd(HS)_2°$ and $Pd(HS)_3^-$ were calculated and preliminary values of the constants of the $PdS_{(cr)}$ dissolution reactions with the formation of these complexes ($K°_{Pd(HS)_2°}$; $K°_{Pd(HS)_3^-}$) were obtained on their basis. The obtained constants of the reactions in the temperature range of 4 – 490°C were fitted to the density model equation which can be used to predict the solubility of Pd-bearing minerals up to 700 °C, 2000 bar.

Keywords: palladium, solubility, hydrothermal fluids, experiment, sulfide complexes

1. Introduction

Palladium is a noble metal and one of the platinum-group metals (PGE). Palladium finds use in electronics, medicine, mechanical engineering, and is also used as a catalyst in chemical industry. The source of palladium is magmatic and hydrothermal deposits, which are formed with the participation of aqueous fluids. The aim of this work is to experimentally determine the composition and stability of palladium complexes in sulfide hydrothermal fluid.

Palladium is transported in hydrothermal fluids as chloride and hydrosulfide complexes. (Gammons, Bloom, 1993) conducted experiments on the dissolution of palladium sulfide at temperatures of 30-300°C and interpreted the results using two hydrosulfide complexes $Pd(HS)_2°$ and $Pd(HS)_3^-$. In (Pan et al., 1994), the dissolution of palladium sulfide is described by the formation of only a neutral complex at temperatures of 200–350°C and saturated vapor pressure. According to (Tagirov and Baranova, 2009; Tagirov et al., 2013), the stability of hydrosulfide complexes $Pd(HS)_2°$, $Pd(HS)_3^-$ and $PdS(HS)_2^-$ decreases with increasing temperature, and the role of these complexes in hydrothermal processes is limited to low temperature conditions (t < 100°C). The purpose of this work is to refine the scheme of Pd complex formation in sulfide hydrothermal fluids and to obtain the stability

constants of Pd hydrosulfide complexes in a wide temperature range.

2. Experimental

The experiments were performed according to the classical autoclave method (450 and 490 °C) and the ampoule method (4, 25 and 75 °C) with the determination of the content of the dissolved component after the experiment was quenched.

2.1 The experiments at 4, 25 and 75 °C

Experiments at temperatures below 100 °C were performed using an ampoule method that was described in (Tagirov, Baranova, 2009). Synthetic $PdS_{(cr)}$ and solutions were placed in ampoules that were hermetically sealed and kept until stationary solubility at the required temperature was attained. At the end of the experiment, ampoules were opened, solutions were extracted, filtered, and concentrations of sulfide sulfur and Pd, as well as the pH values were determined.

2.2 The experiments at 450 and 490°C

For experiments at supercritical temperatures and a pressure of 1000 bar, titanium autoclaves (VT-8 alloy) ~ 20 cm^3 were used. The inner surface of the autoclaves was preliminarily passivated with 10% HNO_3 solution at 450 °C and 1000 bar. In the upper part of the autoclave, synthetic $PdS_{(cr)}$ was placed in a titanium container. Solutions for the experiments were prepared on the basis of distilled degassed water or solution of NaOH (volume ~10-17 cm^3). Hydrogen sulfide was introduced into the experimental system by reacting Al_2S_3 with water during the autoclave heating. The composition of the solutions varied from slightly acidic (0.1-2.0m H_2S) to neutral and alkaline (0.02-0.4m H_2S + 0.05-0.4m NaOH). The pressure was set by the degree of autoclave filling with the solution. The filled autoclaves were placed in a preheated oven. The temperature was measured with a nichrosil-nisil thermocouple (Obninsk Thermoelectric Co.), calibrated at the enterprise, and maintained with an accuracy of ±1°C. The duration of the experiments ranged from 9 to 11 days. At the end of the experiment, the autoclaves were quenched in cold water. The condensate was withdrawn from the autoclave. An empty autoclave was filled with aqua regia and placed on a warm electric stove where it was kept for 0.5 hour. Then the aqua regia was poured from the autoclave into the flask with condensate. Thus, samples were based on 50% aqua regia. The Pd concentrations were determined by ICP-MS, the limit of detection for Pd is 0.3 ppb (taking account for the concentration in blank solutions).

3. Results and discussion

The dissolution of PdS under experimental conditions can be described by reactions:

$$PdS_{(cr)} + H_2S^\circ = Pd(HS)_2^\circ \quad K^\circ_{Pd(HS)_2^\circ}, \qquad (1)$$

$$PdS_{(cr)} + H_2S^\circ + HS^- = Pd(HS)_3^- \quad K^\circ_{Pd(HS)_3^-} \qquad (2)$$

The results of the experiments are presented in Table 1.

Table 1. Composition of experimental solutions and the solubility of Pd.

m, mol·(kg H_2O)$^{-1}$			log m_{Pd}
NaOH	H_2S	HCl	
4 °C/1 bar			
0	0.09	0	-7.37
0	0.09	0.01	-7.94
0.005	0.06	0	-8.40
0.01	0.08	0	-8.00
0.05	0.08	0	-8.77
25 °C/1 bar			
0	0.04	0	-8.57
0	0.07	0.006	-8.07
0.008	0.04	0	-7.70
75 °C/1 bar			
0.0009	0.06	0	-8.33
0.003	0.07	0	-8.57
0.06	0.08	0	-8.00
0.01	0.08	0	-7.09
450 °C/1000 bar			
0	0.41	0	-7.06
0	0.59	0	-7.05
0	1.02	0	-6.86
0.06	0.24	0	-6.91
0.23	0.21	0	-6.95
490 °C/1000 bar			
0	0.63	0	-7.93
0	0.99	0	-7.51
0	1.94	0	-7.13
0.06	0.40	0	-7.25
0.19	0.43	0	-6.64
0.42	0.45	0	-6.64

Table 2. Values of Gibbs energy of palladium sulfide complexes and reaction (1) and (2) constants. Our experimental data of this study are combined with the data previously published by Tagirov and Baranova (2009).

Temperature/pressure	$Pd(HS)_2°$		$Pd(HS)_3^-$	
	$\Delta_f G$, kJ/mol	$\log K°_{Pd(HS)_2°}$	$\Delta_f G$, kJ/mol	$\log K°_{Pd(HS)_3^-}$
4 °C /1 bar	-70.9±0.9	-6.8±0.2	-68.0±1.1	-4.9±0.2
25 °C /1 bar	-70.9±0.9	-6.9±0.2	-75.4±0.7	-4.1±0.1
60 °C /1 bar	-65.8±1.3	-8.0±0.2	-80.8±0.7	-4.2±0.1
75 °C /1 bar	-71.1±3.1	-7.3±0.5	-79.6±1.8	-4.7±0.3
200 °C /P_{sat}	-	-	-97.6±0.8	-5.4±0.1
450 °C /1000 bar	-126.6±2.8	-6.8±0.2	-146.8±3.8	-4.7±0.3
490 °C /1000 bar	-123.9±2.9	-7.6±0.2	-145.2±3.1	-5.4±0.2

Speciation calculations were performed with the help of the Gibbs computer code of the HCh software package (Shvarov, 2008). Optimization of the values of the Gibbs energy of palladium complexes was carried out in the OptimA program. Values $\Delta_f G_{T,P}$ of palladium sulfide complexes and reaction constants (1) and (2) are presented in Table 2.

The obtained values $K°_{Pd(HS)_2°}$ and $K°_{Pd(HS)_3^-}$ were used to determine parameters of the density model equation. As a result, the equations were obtained:

$$\lg K°_{Pd(HS)_2°} = -9.63 + 0.729\cdot10^3/T(K)^{-1} - 5.903\cdot\log d(w) \quad , \quad (3)$$

$$\lg K°_{Pd(HS)_3^-} = -5.88 + 0.423\cdot10^3/T(K)^{-1} - 0.492\cdot\log d(w) \quad , \quad (4),$$

where d(w) is the pure water density. We suppose that equations (3) and (4) can be used at temperatures up to 700 °C and pressure up to 2 kbar. The calculation of the density model and experimental data are shown in Fig. 1 together with the data for Pt hydrosulfide complexes from the study (Filimonova et al., 2021). An increase in temperature leads to a slight decrease in the stability of $Pd(HS)_3^-$. For the $Pd(HS)_2°$ complex, there is a slight decrease in stability at t < ~300 °C and an increase at higher temperatures.

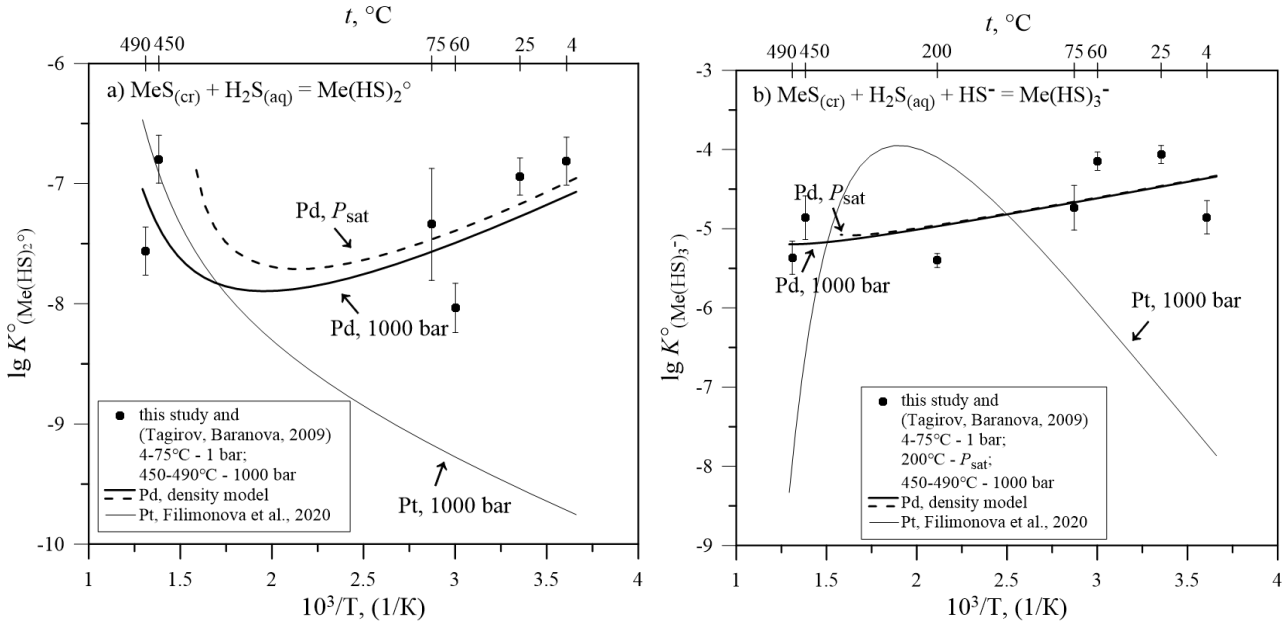

Fig. 1. Log of $MeS_{(cr)}$ solubility constants with the formation of Me–HS complexes as a function of temperature. Points are experimental data; lines were calculated using the density model equation (3, 4).

Conclusions

Based on the results of the experiments, the Gibbs free energies of the $Pd(HS)_2°$ and $Pd(HS)_3^-$ complexes were calculated, and based on them, preliminary values of the $PdS_{(cr)}$ dissolution reaction constants were obtained. It was found that these complexes behave differently depending on *PT*-conditions. The stability of $Pd(HS)_3^-$, which prevails at slightly acidic and near-neutral pH, slightly decreases with increasing temperature. In contrast to the similar $Pt(HS)_3^-$ complex, whose contribution to Pt transport is negligible at $t > 250$ °C, $Pd(HS)_3^-$ is an important form of Pd transport in high-temperature near-neutral solutions, including supercritical fluids.

Stability of $Pd(HS)_2°$ at subcritical temperatures is higher than that of $Pt(HS)_2°$. However, at near-critical and supercritical parameters, the values of the stability constants of these complexes are close. The difference in the dependence of the stability of Pd and Pt complexes on temperature can lead to the separation of these metals in hydrothermal systems. The obtained data will be used to model the hydrothermal transport of palladium during the formation of deposits of this metal.

This study was supported by the Russian Science Foundation grant No. 23-17-00090.

References

Tagirov, B.R., Baranova, N.N. The state of palladium in sulfide hydrothermal solutions: experimental solubility study // Geochem. – 2009. – Int. 47 (12). – P. 1234-1242.

Filimonova O.N., Tagirov B.R., Zotov A.V., Baranova N.N., Bychkova Y.V., Tyurin D.A., Chareev D.A., Nickolsky M.S. The solubility of cooperite PtS(cr) at 25–450° C, Psat–1000 bar and hydrosulfide complexing of platinum in hydrothermal fluids // Chemical Geology. – 2021. – Vol. 559. – P. 119968.

Gammons C.H., Bloom M.S. Experimental investigation of the hydrothermal geochemistry of platinum and palladium: II. The solubility of PtS and PdS in aqueous sulfide solutions to 300°C // Geochim. Cosmochim. Acta. – 1993. – Vol. 57. – P. 2451-2467.

Pan P. and Wood S.A. Solubility of Pt and Pd sulfides and Au metal in aqueous bisulfide solutions II. Results at 200 ~ to 350 and saturated vapor pressure // Mineral. Deposita. – 1994. – Vol. 29. – P. 373-390.

Shvarov Y.A. OptimA, OptimB, OptimC, and OptimS compatible with the Unitherm database, for deriving the thermodymic properties of aqueous species from solubility, potentiometry and spectroscopy measurements // Appl. Geochem. – 2015. – Vol. 55. – P. 17-27.

Tagirov B.R., Baranova N.N., Zotov A.V., Akinfiev N.N., Polotnyanko N.A., Shikina N.D., Koroleva L.A., Shvarov Yu.V., Bastrakov E.N. The speciation and transport of palladium in hydrothermal fluids: Experimental modeling and thermodynamic constraints // Geochimica et Cosmochimica Acta. – 2013. – Vol. 117. – P. 348 – 373.

Setkova T.V.[1], Balitsky V.S.[1], Golunova M.A.[1], Balitskaya L.V.[1], Bublikova T.M.[1], Lakhova A.I.[2], Petrov S.M.[2] Interaction of hydrothermal solutions with domanic rock of Alekseevskoe deposit, experimental studies using synthetic aqueous-hydrocarbon inclusions in quartz *UDC: 553.985*

[1]D.S. Korzhinskii Institute of Experimental Mineralogy RAS, Chernogolovka; [2] Kazan National Research Technological University, Kazan setkova@iem.ac.ru

Abstract. The experiments on the interaction of hydrothermal solutions on domanic rock were carried out with simultaneous growth of quartz crystals in the temperature range of 260-550 °C at a pressure of 100 MPa. As a result, the influence of the hydrothermal fluid on the change of the mineral composition of the rock and the character of the organic matter distribution with increasing temperature was shown. The data on the phase composition of fluid inclusions in quartz and in situ thermobarogeochemical study indicate a critically different behavior and phase states of aqueous-hydrocarbon fluids formed by domanic rock at temperatures from 260 to 550 °C. It was found that the most suitable conditions for the generation of petroleum hydrocarbons are the deep Earth areas, where the interaction of domanic rock with hydrothermal solutions takes place in the temperature range of 310-360 °C at a pressure of about 100 MPa.

Keywords: petroleum hydrocarbons, quartz, synthetic inclusions, hydrothermal fluid, solid bitumen

It is widely known that bituminous rocks can serve as a source of petroleum hydrocarbons to replenish depleted and exhausted oil and gas fields (Kayukova et al., 2021; Muslimov and Plotnikova, 2018; Balitsky et al., 2020). The ability of a rock to generate petroleum hydrocarbons is directly related to its mineral composition and the amount of kerogen (mobile organic matter) it contains. The domanic rock of the Alekseevskoye field contains mobile hydrocarbons and is a typical oil source rock. The rock is composed mainly of Upper Devonian siliceous-argillaceous carbonate deposits, occurs at depths of about 1906 m and is characterized by a high organic matter content. In turn, synthetic fluid inclusions in minerals, formed during the simultaneous interaction of supercritical aqueous fluids with bituminous rocks, make it possible to trace in situ changes in the phase composition and phase states of liquid and gaseous hydrocarbons using microthermometry methods, and thus to characterize their stability and migration patterns, as well as to assess the maximum depth of they bedding in the Earth's interiors and the degree of thermometamorphic transformation.

Experiments on the interaction of hydrothermal solutions with domanic rock were carried out with simultaneous growth of quartz crystals according to a previously developed method (Balitsky et al., 2016, Balitsky et al., 2020) in a wide temperature range from 260 to 550 °C at a pressure of 100 MPa. The experiments used solutions with a composition of 7 wt% $NaHCO_3$ and lasted 14 days.

At the end of the experiments, the morphology of the rock surface was studied by optical (ADF) and electron scanning microscopy (Tescan Vega II XMU). The composition of the initial and newly formed mineral phases was determined by electron probe microanalysis (Tescan Vega II XMU with an INCA Energy 450 energy dispersive spectrometer),

and the phases were identified by X-ray analysis on a Bruker D8 ADVANCE.

The distribution of organic matter over the initial rock is characterized by a uniform banded structure throughout the sample (Fig. 1a). The rock contains quartz, calcite, pyrite, feldspars, predominantly anorthite. After hydrothermal fluid interaction on the rock at a temperature of 260/310°C, organic matter aggregates on the surface in the form of spheres up to 30 μm in size (Fig. 1b). When the temperature of the experiment is increased to 400/450 °C (Fig. 1c), the organic matter is present in the form of lamellar formations. When exposed to a fluid at a temperature of 500/550 °C, the organic matter is completely washed out of the rock (Fig. 1d) and deposited on the bottom of the autoclave in the form of solid bitumen. The change in the mineralogical composition of the rock also depends on the temperature conditions of the hydrothermal impact. In the temperature range of 260 - 450 °C the albite ($NaAlSi_3O_8$) and pyroxene group minerals - aegirine ($NaFeSi_2O_6$) and jadeite ($NaAlSi_2O_6$) - crystallize on the rock surface (Fig. 1b, c). Such a mineral association is formed due to the high activity of sodium when using a $NaHCO_3$ solution. At temperatures above 500 °C, the quartz crystals that make up the rock grow and become larger (Fig. 1d).

Polished plates were prepared from grown quartz crystals for further study of water–hydrocarbon inclusions by optical and thermobarogeochemical methods (Nikon Digital Eclipse C1, THMSG-600 Linkam microthermal chamber).

It has been found that the phase composition of inclusions formed in quartz depends on the temperature. At a low temperature of 260/310 °C, inclusions are formed with a phase composition of L1>G>>L2. Oil inclusions with L2>>L1≥G≥SB are predominantly formed at a temperature of 310°/360°C. At the same time, a large amount of solid bitumen phase was found in the inclusion, on the quartz surface and in the charge, identified as asphaltene by Raman spectra. Inclusions with phase composition L1≥G>L2 formed at a temperature of 400/450°C are larger due to the rapid defective growth of quartz under these conditions. Inclusions formed at high temperatures do not contain the L2 phase of liquid petroleum hydrocarbons, and are represented by the composition G≥L1≥SB with a predominance of solid bitumen.

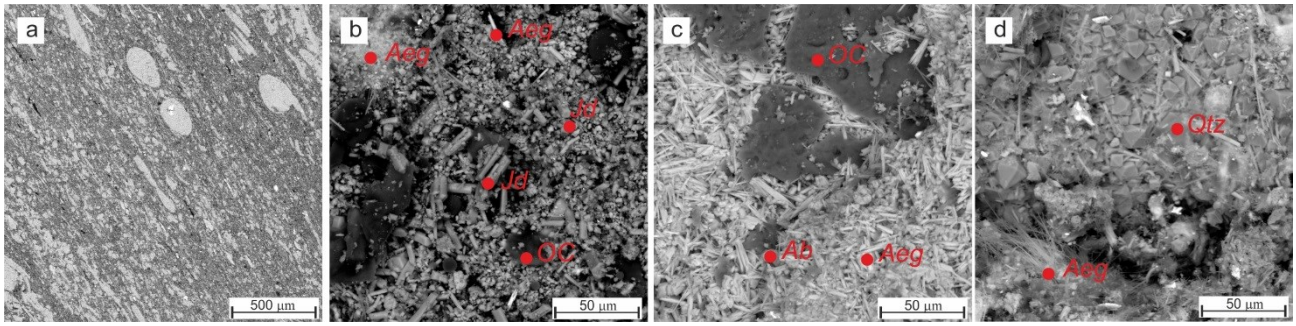

Fig. 1. SEM images of initial rock (a) and rock after hydrothermal fluid interaction (composition 7 wt% $NaHCO_3$) at 260/310 °C (b), 400/450 °C (c), 500/550 °C (d) and a pressure of 100 MPa. Notations: ***OC*** - organic compound, ***Qtz*** - quartz, ***Ab*** - albite, ***Aeg*** - aegirine, ***Jd*** - jadeite. The slash indicates the temperature at the top and bottom of the autoclave.

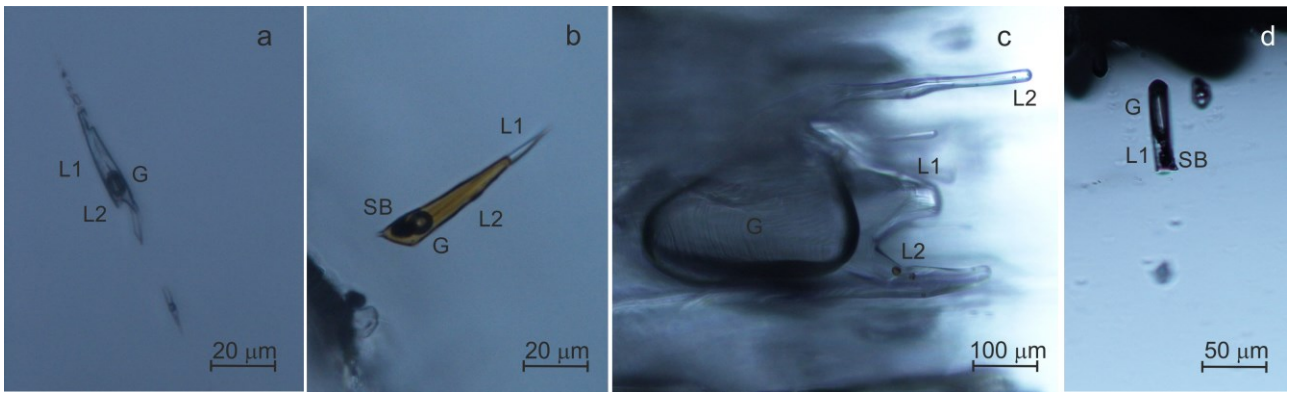

Fig.2. Water-hydrocarbon inclusions in quartz formed at temperatures (a) - 260/310 °C, (b) - 310/360 °C, (c) - 400/450 °C, (d) - 500/550 °C during interaction of hydrothermal fluid with domanic rock. Notations: G – gas, L1 – aqueous solution, L2 – liquid phase of petroleum hydrocarbons, SB – solid bitumen phase.

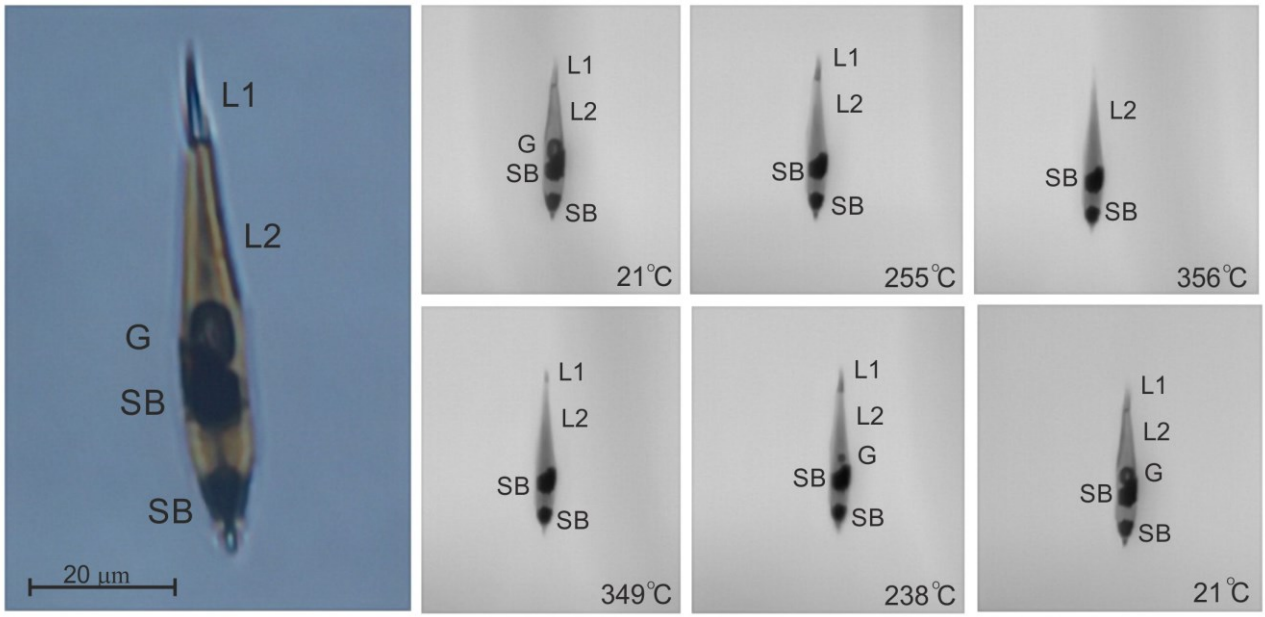

Fig.3. Water-hydrocarbon inclusions in quartz, formed at a temperature of 310/360 °C (left), microthermogram of the inclusion during heating and cooling.

The microthermogram of a predominantly oil inclusion (Fig. 3) shows the sequential dissolution of first the gas phase (G) at 255 °C, then the aqueous phase (L1) at 356 °C. Solid bitumen (SB) does not dissolve, at least up to a temperature of 356 °C. Further cooling of the inclusion leads to the reversible appearance of phases in the same order.

As a result of the experimental study, the influence of the hydrothermal fluid on the change in the mineral composition of domanic rock and the feature of the distribution of organic matter with increasing temperature was shown. Data on the phase composition of fluid inclusions and their in situ study by thermobarogeochemistry indicate to fundamentally different behavior and phase states of water–hydrocarbon fluids formed with the participation of domanic rocks at temperatures from 260 to 550 °C. These differences are due to the cracking of petroleum hydrocarbons that are generated from the rock. The most favorable conditions for their formation are deep areas of the Earth, where domanic rocks interact with hydrothermal solutions in the temperature range of 310–360 °C and at pressures of about 100 MPa.

This study is fulfilled under Research program № FMUF-2022-0003 of the Korzhinskii Institute of Experimental Mineralogy.

References

Balitsky V. S., Penteley S. V., Pironon J., Barres O., Balitskaya L. V., Setkova T. V. Phase states of hydrous–hydrocarbon fluids at elevated and high temperatures and pressures: Study of the forms and maximal depths of oil occurrence in the Earth's interior. Doklady Earth Sciences, 466(2):130–134, 2016.

Balitsky V.S., Setkova T.V., Balitskaya L.V., Bublikova T.M., and Golunova M.A. Phase composition and states of water-hydrocarbon fluids at elevated and high temperatures and pressures (experiment with the use of synthetic fluid inclusions). In Advances in Experimental and Genetic Mineralogy, volume 11 of Special Publication to 50th Anniversary of DS Korzhinskii Institute of Experimental Mineralogy of the Russian Academy of Sciences. Litvin Yu.A. Safonov O.G (Editors), New York, 2020. New York.

Kayukova G.P., Mikhailova A.N., Nasyrova Z.R., Vakhin A.V. Hydrothermal transformations of the organic matter of the rocks of the Domanik deposits of Tatarstan into shale oil - Moscow: "GEOS Publishing House", 2021. 328 p. ISBN 978-5-89118-840-2.

Muslimov R.Kh., Plotnikova I.N. Accounting for the processes of reformation of oil deposits during long-term operation and deep replenishment in modeling the development of oil fields. Georesources. 20(3):186-192, 2018.